REPORT DOCUMENTATION PAGE

Form Approved
OMB NO. 0704-0188

1. AGENCY USE ONLY (Leave Blank)	2. REPORT DATE	3. REPORT TYPE AND DATES COVERED
	30 November 2001	Final Report: 01 Jan 99 - ~~Sept. 1998 - August 2001~~ 31 Dec 99

4. TITLE AND SUBTITLE

Systems Integration of Uncooled YBaCuO IR Detectors

5. FUNDING NUMBERS

38673PH
ARO_MIPR

6. AUTHOR(S)

Donald P. Butler and Zeynep Celik-Butler

7. PERFORMING ORGANIZATION NAME(S) AND ADDRESS(ES)

Southern Methodist University
School of Engineering, Electrical Engineering Department
PO Box 750338
Dallas, TX 75275-0338

8. PERFORMING ORGANIZATION REPORT NUMBER

9. SPONSORING / MONITORING AGENCY NAME(S) AND ADDRESS(ES)

U. S. Army Research Office
P.O. Box 12211
Research Triangle Park, NC 27709-2211

10. SPONSORING / MONITORING AGENCY REPORT NUMBER

38673.19-PH

11. SUPPLEMENTARY NOTES

The views, opinions and/or findings contained in this report are those of the author(s) and should not be construed as an official Department of the Army position, policy or decision, unless so designated by other documentation.

12 a. DISTRIBUTION / AVAILABILITY STATEMENT

Approved for public release; distribution unlimited.

12 b. DISTRIBUTION CODE

13. ABSTRACT (Maximum 200 words)

Infrared imaging has demonstrated itself as a vital aspect of modern weapons systems. Infrared (IR) imaging has the potential to play an equally important role in commercial applications in medicine and transportation. Automobiles equipped with infrared imaging capabilities have been envisioned for the near future. This technology has the potential to tremendously improve personal safety by enabling good vision at night and under adverse weather conditions. Infrared imagers in automobiles may also be an enabling technology for "intelligent super-highways". However, IR imaging systems currently used by the military are too costly for consumer applications. This necessitates the development of inexpensive, uncooled infrared imaging systems that possess high detectivity for night vision applications. This research investigated the integration of semiconducting YBaCuO into micromachined thermal isolation structures to produce uncooled infrared detectors. Various detector structures were developed including a self-supporting structure where the 300 to 400-nm-thick thin film YBaCuO thermometer was held above the substrate by its electrode arms producing a detector with very low thermal mass (as low as 2.3 nJ/K) while maintaining an absorption of 30%. Also dual microcavity detectors were developed for to produce a relatively flat spectral reponse over a large optical bandwidth.

14. SUBJECT TERMS	15. NUMBER OF PAGES
uncooled infrared detectors, YBaCuO	33
	16. PRICE CODE

17. SECURITY CLASSIFICATION OR REPORT	18. SECURITY CLASSIFICATION ON THIS PAGE	19. SECURITY CLASSIFICATION OF ABSTRACT	20. LIMITATION OF ABSTRACT
UNCLASSIFIED	UNCLASSIFIED	UNCLASSIFIED	UL

NSN 7540-01-280-5500

Standard Form 298 (Rev.2-89)
Prescribed by ANSI Std. 239-18
298-102

20020125 278

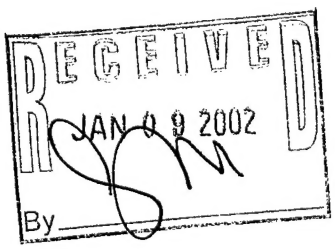

Final Report for Period: 09/1998 - 08/2001
Principal Investigator: Butler, Donald P.
Organization: Southern Methodist Univ
Title:
GOALI: Systems Integration of Uncooled YBaCuO IR Detectors

Submitted on: 11/30/2001
Award ID: 9800062

Project Participants

Senior Personnel

Name: Butler, Donald
Worked for more than 160 Hours: Yes
Contribution to Project:
Prof. Donald Butler shares the full responsibility for the supervision of the project with the Co-PI.

Name: Celik-Butler, Zeynep
Worked for more than 160 Hours: Yes
Contribution to Project:
Prof. Zeynep Celik-Butler shares the full responsibility for the the supervision of the project with the Co-PI.

Post-doc

Name: Leonov, Vladimir
Worked for more than 160 Hours: Yes
Contribution to Project:
Dr. Leonov is a full-time Post-Doctoral Associate working on the project, under the sponsorship of Raytheon Systems Co. As this project is a GOALI, substantial cost-sharing is provided by Raytheon. Dr. Leonov characterized the pyroelectric detector arrays supplied by the company for their responsivity, detectivity, noise, thermal conductance and electrical impedance. Correlation between noise and thermal properties was investigated. During the last phase, Dr. Leonov is going to play a substantial role in integration of the Raytheon Systems with the devices fabricated at Southern Methodist University (SMU).

Graduate Student

Name: Almasri, Mahmoud
Worked for more than 160 Hours: Yes
Contribution to Project:
Mr. Almasri is Ph.D. student fully supportedby the NSF grant. During the past reporting period, he has designed, fabricated and tested different self-supporting, planar and mesa-style YBaCuO microbolometer stuctures. Since no bridge was used in these IR detectors, the thermal mass and therefore the thermal response time is low, making the detectors faster than their conterparts. He also designed another lithography mask set with lower thermal conductance and therefore higher responsivity.

Name: Yaradanakul, Alparslan
Worked for more than 160 Hours: Yes
Contribution to Project:
Mr. Yaradanakul is a Ph.D. student who gives full-time effort to this project. He developed a mirror technology under the microbolometer and suspended pyroelectric IR detector structures to enhance the total IR radiation absorption by the detector. If the cavity under the detector is optimized to wavelength/4, higher sensitivity to that wavelength is achieved. He designed and developed an absorber layer on top of the IR sensitive layer to increase the absorptivity of the pixel.

Name: Yildiz, Ali
Worked for more than 160 Hours: Yes
Contribution to Project:
Mr. Yildiz is a Ph.D. student working on the project. He is fully supported by Southern Methodist University as cost-sharing in the project. During the past reporting period, Mr. Yildiz worked on pulsed laser annealing of IR sensitive materials to obtain high temperature coefficient of resistance and pyroelectric coefficent without inducing damage to the underlying bridge structure and electronics.

Undergraduate Student

Name: Myers, Carissa

Worked for more than 160 Hours: Yes

Contribution to Project:

Ms. Myers is an undergraduate student supported by the NSF-Research Experience for Undergraduates (REU) Supplemental Grant. Her involvement in the project is as a technical support in device imaging using scanning electron microscopy, bonding and initial probing of the finished devices. The initial testing includes visual inspection, resistivity measurements, an varification of response to IR radiation.

Name: Soleimanzadeh, Reza

Worked for more than 160 Hours: Yes

Contribution to Project:

Mr. Soleimanzadeh is an undegraduate student working on the project supported by the NSF-Research Experience for Undergraduates (REU) Supplemental grant. His responsibilities have been assisting Dr. Leonov in characterizing Raytheon detectors and investigating compatibility issues between SMU and Raytheon fabrication processes for integration of two technologies.

Name: Myers, Chad

Worked for more than 160 Hours: Yes

Contribution to Project:

Chad has been working part time as an undergraduate research assistant under the REU supplemental grant. His major contribution has been writing and revising the existing code for the computer programs that control the microprobe stage used in die testing of the IR detectors.

Name: Mcnabb, Fleetwood

Worked for more than 160 Hours: Yes

Contribution to Project:

Fleetwood Wynne McNabb is going to start in June 1, 2000 as an undergraduate summer research assistant. We envision Wynne to spend about a month or two learning about our research program. Towards the second half of the summer, she will be able to contribute as a back-end process engineer: bonding, testing, inspection etc.

Name: Rajan, Venket

Worked for more than 160 Hours: Yes

Contribution to Project:

REU Student: Developed software for a prototype IR camera that uses the IR detectors developed in this investigation.

Research Experience for Undergraduates

Organizational Partners

Raytheon TI Systems

Collaboration with Raytheon TI Systems is multi-facetted. The company provides financial assistance to the project by fully supporting a Post-doctoral associate, partially supporting the PI and Co-PI, and providing funding for some supplies. The PI, Dr. Donald P. Butler, was on sabbatical during Fall Semester 1998 at Raytheon and collaborated with the Company's Uncooled IR Detector group lead by Dr. Charles Hanson. The company provided in-kind support to Dr. Butler in terms of office space, access to laboratory and computational facilities and characterization expertise. Since the ultimate goal of this project is to integrate Raytheon IC Read-Out Circuitry with SMU's detectors, close collaboration at all levels is required.

Collaboration with Raytheon has been strengthened further in the second reporting period. The company provided an additional $23,551to SMU-IR group, bringing the total to $96,222. Dr. Celik-Butler took a sabbatical leave in Fall 2000 , part of which was at Raytheon Systems Company, where sheworked on an rf MEMS project.

Other Collaborators or Contacts

There have been several other collaborators and contacts in the project. Each one is described below:

National Aeronautics and Space Administration (NASA): Drs. Zeynep Ãelik-Butler and Donald P. Butler, were granted a contract by NASA-Langley Research Center to build broadband thermal detector technologies, which will enhance current and future spaceborne Earth radiation measurement instruments. The simultaneous measurement of cloud properties and the radiation fluxes at the top of the atmosphere, at the Earth's surface, and within the atmosphere has been the goal of the Earth Observing System's (EOS's) investigation identified as CERES (Clouds and the Earth's Radiant Energy System). As EOS enters its second generation of instruments and scientific investigations, NASA needs to examine the need for these measurements in the context of the scientific environment of the first quarter of the twenty first century. In this new technology development, we expect to explore needed advances in detector technology that allow a new generation of CERES instruments to measure the radiation in relatively narrow spectral bands that partition the atmospheric and surface energy budget in ways that are not possible with the classic broadband scanners used previously.

This project has lead to a new grant from NASA-Langley to develop broadband far-infrared detectors for a spectrometer. Dr. Zeynep Celik-Butler and Dr. Donald Butler are working with team members from the NASA-Langley, Harvard-Smithsonian Astrophysical Observatory, the Utah State University Space Dynamics Laboratory, and G&A Technical Software to develop the spectrometer under funding from the NASA Instrument Incubator Program. The spectrometer will be used to study the far-infrared spectroscopy of the troposphere. The instrument will enable new, spectroscopic investigation of the earth's radiant energy flux that will help global warming investigations and a greater understanding of climate.

University of Illinois: Leslie H. Allen, Associate Professor of Materials Science has contacted the PIs to collaborate on the use of semiconducting YBaCuO as a micro heater material in their MEMS-based nanocalorimeters. Investigations are underway towards this direction.

University of Texas at Arlington: Dr. Kim at the Department of Materials Science has been very helpful in doing X-ray diffraction analysis for the SMU IR research group. UTA is a partner in MRCEDM (Metroplex Research Consortium for Electronic Devices and Materials) that us described later in this report.

Polish Academy of Sciences, Physics Department: Ph.D. student Andrii Klimov from Polish Academy of Sciences, Physics Department has visited University of Rochester and Southern Methodist University. Mr. Klimov's visit involved the investigation of the optical properties amorphous YBaCuO thin films. Three types of samples were investigated; amorphous, insulating thin films fabricated by PLD at the Polish Academy of Sciences (r~10^7 Ohm-cm), amorphous, semiconducting thin films fabricated by rf sputtering at Southern Methodist University (r~5 Ohm-cm), and epitaxial semiconducting YBaCuO thin films fabricated by PLD at Southern Methodist University (r~1 Ohm-cm). The first two sample types possess short-range structural while the latter possesses long range structural order. The samples are characterized by resistivity versus temperature measurements to determine the conduction mechanism, Hall effect, and optical measurements. The optical measurements include monochrometer studies over the wavelength range of 0.6-12mm. These measurements were performed at SMU. In addition, the transient optical response of the films was characterized at the University of Rochester, Laboratory for Laser Energetics. One of the PIs, Donald Butler, had a long-standing collaborative relationship with Prof. Roman Sobolewski at The Laboratory for Laser Energetics. He has characterized the transient behavior of some semiconducting YBaCuO thin films using ultrafast laser sources at 810 nm and 1060 nm. Prof. Sobolewski has a tunable ultrafast laser that can be tuned from visible to 10mm wavelengths. This range is very interesting for the work at SMU on uncooled IR detectors. Preliminary investigations have resulted in two publications, and provided information about the time constants and temperature dependence of the signal. An investigation of the wavelength dependence of the time constants and the absorption of the films would provide useful information affecting the ultimate performance of semiconducting YBaCuO uncooled infrared detectors. Mr. Klimov worked closely with graduate students and post-doctoral associates at SMU and the University of Rochester to perform the experiments.

University of Rochester, Laboratory for Laser Energetics was a partner in our collaboration with Polish Academy of Sciences. The University of Rochester has also done ultra-fast optical sampling measurements on our YBaCuO thin films, confirming pyroelectricity exhibited by the materials.

Activities and Findings

Research and Education Activities: (See PDF version submitted by PI at the end of the report)

Please refer to the attached activities PDF file.

Findings: (See PDF version submitted by PI at the end of the report)

Please refer to the attached findings PDF file.

Training and Development:

GRADUATE STUDENT TRAINING

A total of three Ph.D. students are trained in all aspects of IR detection and micromachining. These aspects include device and system design, fabrication, testing and data analysis. Mahmoud Almasri has defended his dissertation and has joined General Monitors, CA to take a leading role in their MEMs sensor program. Alp Yaradanakul and Ali Yildez are in the final stage of their Ph.D. studies and are expected to defend their dissertations in the next couple of months. In addition, Ph.D. student Andrii Klimov from Polish Academy of Sciences, Physics Department has visited University of Rochester and Southern Methodist University. Mr. Klimov's visit involved the investigation of the optical properties amorphous YBaCuO thin films. Detailed description is provided in the 'collaborators' section.

UNDERGRADUATE STUDENT TRAINING (NSF-REU'S)

Five undergraduate research assistants, Carissa Myers, Reza Soleimanzadeh, Chad Myers, Fleetwood McNabb, and Venket Rajan, have worked on design, fabrication and testing of IR detectors and microelectromechanical systems. Venket Rajan and Chad Myers have developed the software to power the scanned IR camera developed at SMU.

Outreach Activities:

Metroplex Research Consortium for Electronic Devices and Materials (MRCEDM) was formed in July 1998 between four north Texas Universities: Southern Methodist University, University of North Texas, University of Texas at Arlington and Texas Christian University. Texas Instruments Inc. was an instigator in the formation of the Consortium with a donation of optical and electronic equipment valued at $6M. SMU obtained equipment worth about $600-800K from the Consortium divided between SEAS and Dedman, Department of Chemistry. The equipment is divided between the universities according to field of expertise. Since then, the consortium has submitted three proposals: one declined, one pending and one granted. An operation charter was developed and approved. It was agreed that Texas Engineering Experiment Station (TEES) is going to be the managing partner of MRCEDM. According to the charter, each university and TEES contributes $25,000 to the Consortium. In addition, TEES provided a start-up funding of $50,000. Texas Instruments joined the consortium at the full level of $100,000 per year for a minimum of three years. Tri-Quint Semiconductor joined at $25,000 per year for a minimum of five years. Membership of other companies are under negotiation.

We have developed a 5000/7000 level microelectromechanical systems (MEMS) and devices course that is cross-listed with the Department of Mechanical Engineering. It is offered for the first time in Spring 1999 and annually since. This is a natural extension of the micromachining technology developed in our laboratories through the infrared detection research sponsored through this project. It is modeled after two similar courses offered in the University of California, Berkeley and Princeton University. The course develops the basics for microelectromechanical devices and systems including microactuators, microsensors, and micromotors, principles of operation, different micromachining techniques (surface and bulk micromachining), IC-derived microfabrication techniques, thin-film technologies as they apply to MEMS. The first time it was offered, about 40% of this course was taught by a ME faculty member. In later years, one of the PIs, Dr. Celik-Butler taught the course fully. More information can be found at http://www.seas.smu.edu/ee/5314/.

Journal Publications

D. P. Butler, Z. Ãelik-Butler, R. Adam, and R. Sobolewski, "Pyroelectric Effect in Y-Ba-Cu-O Thin Films Under Laser Illumination", Journal of Applied Physics, p. 1075, vol. 85, (1999). Published

J. Gray, Z. Ãelik-Butler, and D. P. Butler, "MgO Sacrificial Layer for Micromachining Uncooled Y-Ba-Cu-O IR Microbolometers", IEEE Journal of Microelectromechanical Systems, p. 192, vol. 8, (1999). Published

M. Almasri, D. P. Butler, Z. Ãelik-Butler, R. Adam, R. Sobolewski, "Cryogenic Performance of Semiconducting Y-Ba-Cu-O for Infrared Detection", Superconductor Science and Technology, p. 751, vol. 12, (1999). Published

A. Yaradanakul, Z. Ãelik-Butler, and D. P. Butler, "Room Temperature Semiconducting YBaCuO Microbolometers with Ti Absorber", International Journal of Advanced Manufacturing, p. 13, vol. 3, (2000). Published

V. Leonov, D. P. Butler, Z. Ãelik-Butler, K. R. Udayakumar, C. M. Hanson, and H. R. Beratan, "Dielectric loss and related noise of pyroelectric modified lead titanate arrays", Solid State Electronics, p. 735, vol. 45, (2001). Published

M. Almasri, D.P. Butler, and Z. Ãelik-Butler, "Self-supporting Semiconducting Y-Ba-Cu-O IR Microbolometers", IEEE/ASME Journal of Microelectromechanical Systems, p. 469, vol. 10, (2001). Published

V. Leonov and D.P. Butler, "Two-color Thermal Detector with Thermal Chopping for Infrared Focal Plane Arrays", Applied Optics, p. 2601, vol. 40, (2001). Published

A. Yildez, Z. Ãelik-Butler, D.P. Butler, and C.-U. Kim, "Investigation of the Temperature Coefficient of Resistance and Crystallization of YBaCuO Thin Films Using Pulsed Laser Annealing", Journal of Vacuum Science and Technology B, p. , vol. , ( ). Submitted

M. Almasri, D.P. Butler, and Z. Ãelik-Butler, "Broad-Band IR Microbolometers for Space Applications", IEEE/ASME Journal of Microelectromechanical Systems, p. , vol. , ( ). Submitted

Books or Other One-time Publications

Z. Ãelik-Butler and D. P. Butler, "Uncooled IR Detector Arrays", (1998). Book, Published
Editor(s): John G. Webster
Collection: Wiley Encyclopedia of Electrical and Electronics Engineering
Bibliography: ISBN: 0-471-13946-7

R. Sobolewski and D.P. Butler, "Infrared Optical Sensors", (2001). Book, Accepted
Editor(s): D. Cardwell and D. Ginley
Collection: Handbook of Superconducting Materials (Chapter 5.2)
ISBN: 0-750-30432-4
Bibliography: Editors-in-chief Institute of Physics, Bristol, UK, BS1 6BE

D. P. Butler, Z. Ãelik-Buter and R. Sobolewski, "Yttrium Barium Copper Oxide as an Infrared Sensing Material", (2000). Book, Published
Editor(s): H. S. Nalwa
Collection: Handbook of Advanced Electronic and Photonic Materials
ISBN:0-12-513745-1
Bibliography: Academic Press 2000

M. Almasri, D. P. Butler, and Z. Ãelik-Butler, "Free Standing Amorphous Semiconducting YBaCuO Detectors for Uncooled IR Detection and the Effects of Doping", (1999). Conference Proceeding, Published
Editor(s): Randolph E. Longshore
Collection: Proceedings of SPIE vol. 3794, Growth and Characterization of Materials for Infrared Detectors III
Bibliography: SPIE 44th Annual Meeting, 18-23 July 1999, Denver, Co.

Mahmoud Almasri, Donald P. Butler, Zeynep Celik-Butler, Roman Adam,
and Roman Sobolewski, "Cryogenic Performance of Semiconducting Y-Ba-Cu-O for Infrared Detection", (1999). Conference Proceedings, Published
Editor(s): Stephen Whiteley
Collection: International Superconductive Electronics Conference, Superconductor Science and Technology
Bibliography: (ISEC'99) Berkeley, CA, June 21-26, 1999

Roman Adam, Roman Sobolewski, Zeynep Ãelik-Butler and Donald P. Butler, "Uncooled Y-Ba-Cu-O detectors based on the pyroelectric and bolometric effects", (1999). Conference Proceedings, Published
Bibliography: 1999 International Workshop on Superconductivity (4th Joint ISTEC/MRS Hawaii Workshop), Kauai, Hawaii, 27-30 June 1999

D. P. Butler and Z. Celik-Butler, "Uncooled YBaCuO Microbolometers for Advanced Broad-Band IR and FIR Radiation Detection", (2000). Conference Proceedings, Published
Collection: Proceedings of NanoSpace 2000 (CD-ROM)
Bibliography: NanoSpace 2000,League City, Texas. January 23 - 28, 2000

R. Sobolewski, D. P. Butler, Z. Ãelik-Butler, "Cooled and uncooled Infrared detectors based on Yttrium Barium Copper Oxide", (2000). Conference proceedings, Published
Collection: Proceedings of International Conference on Advanced Optical Materials and Devices, SPIE 4318, p.204
Bibliography: Vilnius, Lithuania, August 16 - 19, 2000.

D. P. Butler, M. Almasri, and Z. Celik-Butler, "Semiconducting YBaCuO Bolometers for Uncooled IR Detection", (2000). Conference Proceeding, Published
Editor(s): E. L. Dereniak
Collection: SPIE Proceedings, SPIE 4028, 17-26
Bibliography: 14th SPIE Annual International Symposium on Aerospace/Defense Sensing, Simulation and Controls: Infrared Detectors and Focal Plane Arrays VI, Orlando, FL, 24-28 April, 2000.

28. Donald P. Butler, Zeynep Ãelik-Butler, Mahmoud Almasri, Alp Yaradanakul, Ali Yildiz, "Uncooled Microbolometers Based on Semiconducting YBaCuO for Broad-Band IR Radiation Detection", (2000). Conference Proceedings, Published
Collection: NanoTech 2000, Houston, TX, Sept. 24-28 2000
Bibliography: Proceedings of the Nanotech 2000 Conference

Z. Ãelik-Butler, D. P. Butler, M. Almasri, A. Yardanakul, A. Yildiz, "YBaCuO microbolometers for broad-band IR sensing", (2001). Conference Proceedings, Published
Editor(s): B.F. Andresen, G.F. Fulop, and M. Strojnik
Collection: SPIE Aerosense, Infrared Technology and Applications XXVII, Orlando, FL, April 2001
Bibliography: SPIE 4369, pp. 264-273 (2001)

Web/Internet Site

URL(s):
http://www.engr.smu.edu/~dpb/detectors/index.html
Description:
Provides information on our research on uncooled infrared detection

Other Specific Products

Product Type: PATENTS
Product Description:
Patent #1 'Uncooled YBaCuO Thin Film Infrared Detector', by Donald P. Butler, Zeynep Ãelik-Butler, and Pao Chuan Shan, Filed Feb. 1, 1995, granted November, 1996. Patent #: 5572060.

Sharing Information:
All patents are assigned to Research Corporation Technologies Inc. and are available for licensing.

Product Type: PATENTS
Product Description:
Patent #2. 'Amorphous YBaCuO Thin Film Infrared Bolometer for Uncooled Infrared Detection', by Donald P. Butler, Zeynep Ãelik-Butler, Pao Chuan Shan, and Agha Jahanzeb, Filed June 22, 1995, granted October 13, 1998. Patent #: 5821598.
Sharing Information:
All patents are assigned to Research Corporation Technologies Inc. and are available for licensing.

Product Type: PATENTS
Product Description:
Patent #3. 'Uncooled YBaCuO Thin Film Infrared Detector (Divisional Application for Pyroelectric Effect)', by Donald P. Butler, Zeynep Ãelik-Butler, and Pao Chuan Shan, Filed Feb. 26, 1996, granted September 30, 1997. Patent #: 5672903.
Sharing Information:
All patents are assigned to Research Corporation Technologies Inc. and are available for licensing.

Product Type: PATENTS
Product Description:
Patent #4. 'Uncooled Amorphous YBaCuO Thin Film Infrared Detection', by Donald P. Butler, Zeynep Ãelik-Butler, Pao Chuan Shan, and Agha Jahanzeb, filed May 29, 1998, granted December 15, 1998. Patent #: 5850098.

Sharing Information:
All patents are assigned to Research Corporation Technologies Inc. and are available for licensing.

Contributions

Contributions within Discipline:
Up to the '90s, IR detection has been almost exclusively used and funded by the department of defense as a night vision tool for national security. In this era, cryogenic IR detection with high sensitivity and fast response was emphasized with relatively less concern about the cost. Most of the research and development were done in 'secured environments' at national laboratories and companies with very little or no contribution from universities. Recently, as defense expenditures are decreased, and dual-technology (defense and commercial) based research is emphasized, these companies started to search for commercial applications of IR detection and found plenty, ranging from intruder detection to night-time navigation in automotive industry, from biomedical imaging to forest fire detection. Since the commercial market is very cost-sensitive, a need developed for room temperature IR detection without expensive cryogenics. The industry was looking for an IR sensitive material that is fully compatible with the existing semiconductor fabrication process, that can be operated at room temperature and still be able to perform at a reasonable level for commercial applications. Our patented invention on the bolometric and pyroelectric IR detector using Yttrium Barium Copper Oxide (YBaCuO) thin films provided an answer to that search.
Our patents have been assigned to Research Corporation Technologies Inc. The patents are available for licensing.

Contributions to Other Disciplines:
The PIs were co-organizers of the second Texas Area Workshop on Microelectromechanical Systems (TEXMEMS) that took place on May 16th, 2000 on SMU Campus. TEXMEMS workshops are one-day meetings, whose existence emerged from the notion that most Micro-Electro-Mechanical Systems (MEMS) related academic and technical advances are centered on the West and the East Coasts. Because of the different industries located in Texas, we feel that a third pole should emerge in the Southwest. The one day meeting program encourages interaction and dialog among scientists and engineers to foster developments in MEMS related activities at different levels: Design, Simulation, Fabrication and Applications. TEXMEMS I took place on August 23, 1999 at Texas A&M University, and it was attended by more than 100 people.

The TEXMEMS Workshop II is focused on fostering a technical information exchange between scientists and engineers from different organizations in the Southwest. The meeting is open to everyone who is interested in MEMS. The purpose is to promote dialog and possible collaborations among the scientific and technical communities with prime interest and active research in MEMS. We expect researchers from different communities to meet at this workshop. Presently, MEMS have found applications in several engineering fields as well as the biomedical sciences. It is expected that the growth of these technologies come from the cross-fertilization of ideas enabled by this type of meeting. The format of the meeting is designed to fit in one day so that interested parties (researchers, engineers, university faculty and graduate students) from other institutions can attend the meeting without extra accommodation expenses. It is expected that future TEXMEMS workshop meetings should be held cyclically every six months in cities with large academic and governmental bodies (Houston, Dallas, Austin, College Station).

About 170 scientists and engineers attended TEXMEMS II. The key-note speaker was Dr. Bill Tang, the program manager of MEMS at DARPA. There were 22 contributed papers. In addition, the following invited speakers gave presentations:
À Dr. Steve Rodgers of Sandia National Laboratories
À Dr. Michael A. Mignardi of Texas Instruments
À Dr. Chuck Goldsmith of Raytheon Systems Co.
The technology that this project is based on is the well-known microelectromechanical systems (MEMS) technology. The micromachining techniques developed to achieve low-thermal conductance in the focal plane array of the IR camera can be used in other MEMS applications, including molecular separation, analysis and synthesis applications in bio-MEMS, and micro-valves, micro-actuators and gears in mechanical engineering.
The PIs were involved in the organization of TEXMEMs III in June 2001. The workshop was attended by more than 200 scientists and engineers.

Dr. Donald Butler and Dr. Zeynep Celik-Butler are both Distinguished Lecturers for the IEEE Electron Device Society. Dr. Butler has given 2 lectures related to the work supported by this project and Dr. Celik-Butler has given one. Dr. Butler was also Symposium Chair for the IEEE Emerging Technologies Symposium on Broadband Communications for the Internet Era. The symposium was attended by more than 140 engineers. He is also involved in the establishment of the Texas Nanotechnology Initiative (TNI). A group of University faculty and industrial scientists and engineers who are seeking to promote nanotechnology in Texas. TNI is organizing a conference for March 2002 (NanoVentures).

Contributions to Human Resource Development:
Three Ph.D. students are trained through this project, two supported by NSF, one supported by SMU as a part of cost-sharing.
The project made a contribution to the diversity of the human resource pool for science and technology through the REU program, where most of the undergraduate students are chosen from the underrepresented groups in engineering as defined by the National Science Foundation

(minorities, women and persons with disabilities). Carissa Myers and Fleetwood W. McNabb are female undergraduate students supported by the REU supplement to this NSF grant.

Contributions to Resources for Research and Education:

The contributions to information resources for science and technology have been in the form of developing new design, fabrication and testing methods in IR technology and widely disseminating the results to colleagues in other universities and companies including Raytheon.

The contributions to physical resources for science and technology have been high performance uncooled infrared detectors that have applications in radiometry, spectroscopy and imaging with IR cameras that can be used for production inspection, security, medical sensing etc. A laboratory camera is near completion at SMU.

The contributions to institutional resources for science and technology have been in the form of education and financial support of Ph.D., undergraduate students, and a post-doctoral associate. In addition, the formation of Metroplex Research Consortium for Electronic Devices and Materials (MRCEDM) will benefit the University, in enhanced research activities, better outreach in education and technology transfer. Currently, there are two corporate members of MRCEDM. Two more memberships are pending. The Consortium will provide direct commercialization avenues for the project. Dr. Donald Butler spent a sabbatical semester at Raytheon in Fall 1998. Dr. Celik-Butler spent a two-semester sabbatical split between Raytheon, DRS, and the University of Florida in the 2000-01 academic year.

Contributions Beyond Science and Engineering:

Infrared (IR) imaging has demonstrated itself as a vital aspect of modern weapons systems. IR imaging has the potential to play an equally important role in commercial applications in medicine and transportation. Automobiles equipped with infrared imaging capabilities have appeared with year 2000 model Cadillacs. This technology has the potential to tremendously improve personal safety by enabling good vision at night and under adverse weather conditions. Infrared imagers in automobiles may also be an enabling technology for 'intelligent super-highways'. However, cooled IR imaging systems currently used by the military are too costly for consumer applications. This necessitates the development of inexpensive, uncooled infrared imaging systems that possess high detectivity for night vision applications. Uncooled infrared cameras developed to date have demonstrated good performance at a significantly lower cost than their cooled counterparts. Their performance can still be improved by orders of magnitude to the background limit and their cost is less expensive rather than inexpensive. Cadillac utilizes bulk BaSrTiO pyroelectric detectors that are thinned and attached to the readout circuit by bump-bonding. This is a labor-intensive process. A thin film deposition process is better suited to low-cost, high volume microelectronics manufacturing. Additional contributions are as IR detecting components in medical imaging systems for diagnosis and treatment, in manufacturing environments for failure detection, and in surveillance systems for security among other civilian uses.

Categories for which nothing is reported:

II. ACTIVITIES AND FINDINGS

II-1 Major Research Activities:

II-1A. PROJECT ABSTRACT

Infrared imaging has demonstrated itself as a vital aspect of modern weapons systems. Infrared (IR) imaging has the potential to play an equally important role in commercial applications in medicine and transportation. Automobiles equipped with infrared imaging capabilities have been envisioned for the near future. This technology has the potential to tremendously improve personal safety by enabling good vision at night and under adverse weather conditions. Infrared imagers in automobiles may also be an enabling technology for "intelligent super-highways". However, IR imaging systems currently used by the military are too costly for consumer applications. This necessitates the development of inexpensive, uncooled infrared imaging systems that possess high detectivity for night vision applications.

This proposal concerns the investigation and development of high detectivity pyroelectric infrared imagers operating at room temperature. Previous work supported by the National Science Foundation and Army Research Office has shown that semiconducting, thin film YBaCuO possesses a high pyroelectric coefficient at room temperature, two hundred times greater than other thin film materials. This enables high detectivity pyroelectric thermal detectors to be fabricated on micromachined thermal isolation structures integrated on CMOS read-out circuitry, since the amorphous semiconducting phase of YBaCuO, used in these imaging devices, is deposited at ambient temperature with no need of high temperature post-annealing. It has been demonstrated by researchers at Southern Methodist University (SMU) that surface-micromachined Nb/YBaCuO/Nb capacitor structures are capable of exhibiting pyroelectric coefficients in the range of 65-nC/K cm^2 without an externally applied electric field and in the absence of prior poling. When poled, the pyroelectric coefficient was found to increase to 18 $\mu C/cm^2$-K. If integrated with state-of-the-art thermal isolation structures, background limited performance is achievable as defined by high specific detectivity, in the order of 10^{10} cm-$Hz^{1/2}$/W, and low noise equivalent temperature difference of around 2 mK. This performance would surpass all other uncooled IR cameras.

YBaCuO is best known as a high temperature superconductor. The optical and electronic properties of $YBa_2Cu_3O_{6+x}$ are determined by its oxygen stoichiometry. For $x \approx 1$, YBaCuO possesses an orthorhombic crystal structure, exhibits metallic conductivity, and becomes superconductive upon cooling below its critical temperature. As x is decreased to 0.5, the crystal undergoes a phase transition to a tetragonal structure and it exhibits semiconducting conductivity characteristics as it exists in a Fermi glass state. As x is decreased further below 0.3, YBaCuO becomes a Hubbard insulator with a well-defined energy gap on the order of 1.5 eV. This work utilizes the *semiconducting* phase of the material. SMU researchers have done extensive investigations into the electrical and optical properties of the material and have over 15 publications and presentations, and four patents on the subject.

In this work, high detectivity pyroelectric imagers will be fabricated by combining the SMU pyroelectric devices with the state-of-the-art thermal isolation structures and read-out circuitry produced by Raytheon/TI Systems. Formerly, a part of Texas Instrument Inc., the Defense Systems and Electronics Group has recently been acquired by Raytheon to form Raytheon/TI Systems (RTIS). Both the RTIS and SMU are in Dallas, Texas, in close proximity with each other, making such collaboration very convenient. Two groups in RTIS, in conjunction with SMU principal investigators, will integrate the device concepts developed at the University with TI's imaging systems that were originally developed for their Barium Strontium Titanate pyroelectric detectors.

Various issues at the systems level must be addressed and solved including process compatibility, electrical compatibility, and system figures of merit. To solve the electrical compatibility issue, the resistive loss of YBaCuO will be decreased by adjusting its oxygen content. Process compatibility issue will be addressed by finding an appropriate electrode metal for YBaCuO that is CMOS compatible and designing a fabrication process that incorporates the principles of YBaCuO deposition and lithography with micromachining technology developed for the thermal isolation structures at Raytheon/TI Systems. Several figures of merit, such as pyroelectric coefficient, pyroelectric figure of merit, responsivity, specific detectivity, noise, will be used to assess performance at the focal plane array level. The pyroelectric properties and the noise mechanisms, which limit the detectivity and are uniquely characteristic of the high

degree of thermal isolation, will be investigated. Upon successful completion of integration at the focal plane array level, a systems integration will be attempted towards a complete IR camera. Systems level figures of merit, such as noise equivalent temperature difference, will be used as a measure of performance.

The basic material and device level stages of this work have been sponsored by a previous grant from NSF and ARO. The proposed work will realize a full range of engineering processes from basic research to device concepts to systems integration, thereby developing a complete uncooled IR imager, unsurpassed in performance and cost.

II-1B. OBJECTIVES AND TASKS:

The objective of this project is to develop the next generation Infrared (IR) cameras based on uncooled YBaCuO detectors developed under a previous grant sponsored by NSF and Army Research Office (ARO). At present, most infrared imaging detectors are photon detectors based upon HgCdTe, which must operate at cryogenic temperatures. The necessity of cryogenic cooling significantly increases the system cost beyond a level suitable for many consumer applications in transportation, security, and medicine. Cryogenic photon detectors are therefore used primarily by the military for nightvision and target seeker applications. [1,2]

Tasks:

Task 1. YBaCuO that is compatible with Raytheon/TI Systems' readout circuitry will be fabricated. It is very expensive to redesign a readout circuitry for a focal plane array, therefore it is advantageous to be able to utilize an existing design. To this end, the resistivity of the pyroelectric YBaCuO needs to be increased by fabricating thin films with a slightly reduced oxygen concentration. In YBaCuO, oxygen serves to donate carriers to the mobility band. Sputtering from a target with a lower oxygen concentration should accomplish this objective. However, to first explore the stoichiometry parameters required to achieve the desired resistivity range, it is proposed to use pulsed laser deposition (PLD) to fabricate high resistivity thin films and characterize their pyroelectric behavior by measuring the pyroelectric coefficient and impedance versus temperature using the substrate ramping technique. The PLD system utilizes inexpensive one-inch targets, which can be fabricated in-house by the solid-state reaction technique. Since, similar pyroelectric behavior has been observed in lower resistivity thin films, increasing the resistivity is not expected to alter the pyroelectric behavior significantly. The PLD system can also be used to test the compatibility of YBaCuO with desired electrode materials such as NiCr, tungsten and titanium. Once, the oxygen stoichiometry of the film is determined that provides the optimum target resistivity, the process will be transferred back to sputtering from an oxygen depleted target. Sputtering is more common as an inexpensive deposition technique suitable for low cost manufacturing.

Task 2. Pyroelectric YBaCuO detector arrays will be fabricated on thermal isolation structures jointly by SMU and RTIS. Raytheon/TI Systems will provide substrates to SMU that have been completed up to the point of deposition of the pyroelectric thin film. SMU will deposit the YBaCuO pyroelectric material that has been made compatible with RTIS's readout circuitry. RTIS will complete the fabrication of the pyroelectric detectors in thermal isolation structures. SMU will characterize the devices for their noise properties, pyroelectric properties, infrared responsivity and detectivity.

Task 3. Raytheon/TI Systems will provide SMU with thin film PLZT pyroelectric detectors that they are currently developing for imaging applications. SMU will perform noise studies on the devices and characterize their responsivity and detectivity. The noise will be measured under varying thermal conductance conditions by changing the atmospheric pressure surrounding the device mounted in a cryostat (vacuum chamber). The noise measurements will reveal the dependence of the temperature fluctuation noise on the thermal conductance until the point is reached that only the effects of Johnson noise and background noise dominate. The results will be shared with RTIS.

Task 4. The characteristics of YBaCuO and PLZT pyroelectric imagers will be evaluated for integration with read-out circuitry to produce complete IR Imaging Cameras. The parameters of merit, such as noise equivalent temperature difference, will be measured at the systems level. Focal plane arrays will be fabricated (most likely 300x300 arrays made of 40x40 μm^2 pixels) on finished CMOS wafers with read-out circuitry, using a sacrificial layer.

II-1C. MAJOR ACTIVITIES IN TASK 1 AND TASK 2:

Two major improvements have been incorporated into the design of the detectors. The first one is the self-supporting structures (no bridge) in order to decrease the thermal capacitance, thus allowing thermal conductance to decrease without sacrificing from the frequency response. The second one is the use of absorption layer and a $\lambda/4$ resonant cavity under the bridge to increase absorptivity in the mid-IR region.

Self-supporting IR Detector Structures:

The microbolometers are fabricated in a novel self-supporting structure. The key feature of the structure is that only the metal electrode arms support the YBCO thermometer. No other material is used as a supporting membrane in the structure. This leads to a reduction in the thermal mass of the microbolometer that can be used to achieve a higher thermal cutoff frequency or may be traded off to achieve a higher responsivity and detectivity by further reducing the thermal conductance. These microbolometers are fabricated with a conventional polyimide sacrificial layer to further demonstrate the compatibility of YBCO thermometers with post-CMOS micromachining technology. This will lead to

- simplified fabrication process for higher yield and lower cost
- elimination of stress balancing problems between thin films layered on the bridge
- better CMOS compatibility due to use of titanium for electrode arms
- reduced number of process steps due to use of polyimide mesa structures instead of undercut methods for micromachining
- the opportunity of studying the optical properties of YBaCuO thin films without interference from the underlying films.
- significant reduction in the thermal mass of the suspended thermometer by eliminating the supporting membrane producing a corresponding decrease in response time.
- demonstrated the relatively strong, broadband absorption of semiconducting YBCO due to its Fermi glass band structure.
- A transverse split electrode, pyroelectric detector was demonstrated, reducing the problem associated in obtaining a strong absorption in parallel plate capacitor structures

The results are presented in the Major Findings Section.

High Absorptivity Resonant Detector Structures:

In order to increase the absorptivity, a titanium absorber layer is used on the IR sensitive film. In addition, a resonant cavity is employed under the pixel tuned to quarter of the IR wavelength, $\lambda/4$. For comparison, similar structures are built directly on a substrate without using any micromachining techniques. The results are presented in the Major Findings Section.

Laser Annealing of YBCO thin films:

To increase the resistivity and improve the pyroelectric properties of semiconducting YBCO, pulsed laser annealing of YBCO films in vacuum with a 248-nm excimer laser was investigated. Pulsed laser annealing was observed to increase the resistivity and TCR, as well as increase the average grain size in the polycrystalline films. In some cases, the pyroelectric coefficient was also observed to increase. Similar behavior was observed in YBCO thin films deposited by rf magnetron sputtering onto heated substrates. The pyroelectric behavior of YBCO still fluctuates greatly in its magnitude from being unobservable to relatively strong. Crystallinity appears to be required for pyroelectric behavior with a grain size that must approach at least 10 nm. Mechanical strain has been observed to enhance pyroelectric behavior. The results are presented in the Major Findings Section.

Broadband Detector Structures with Dual Resonant Cavities:

In spectroscopy and radiometric applications, broadband IR and far-IR detectors with relatively uniform absorption over a large optical bandwidth are desired. To develop microbolometers that will satisfy this demand a novel 2-mirror, 2-resonant cavity design was developed. The results are presented in the Major Findings Section.

Micromachined, Two-color Infrared Detectors with Thermal Chopping:

Thermal detectors can be improved by providing a tunable wavelength response and by incorporating a thermal chopper into the detector by using microelectromechanical (MEM) elements. Most thermal detectors require a chopper, continuous synchronous chopping in the case of pyroelectric detectors or asynchronous chopping in the case of staring microbolometers. Mechanical choppers are bulky and costly. This work theoretically investigated the fundamental principals of micromachined thermal detectors that possess tunable wavelength or color response and a technique for thermal chopping. A micromirror, switching between two spatial positions under the detector, provides a response to two wavelength windows by tuning the optical resonant cavity. The image can then be integrated at the read-out level to achieve a multi-color infrared picture. A thermal MEM-chopper can be used instead of mechanical chopper to maintain the same video frame rate and allow for an interlaced resetting of staring thermal arrays. Unlike 2^{nd} generation of uncooled infrared arrays, the actual temperature of objects can be obtained by comparing the response in two wavelength windows, in addition to the direct measurement of infrared power they radiate in entire 8-14 μm spectral region. The results are presented in the Major Findings Section.

Unfortunately, the Raytheon thin film pyroelectric detector program was terminated and the Raytheon group was dissolved before SMU was able to collaborate with Raytheon to fabricate YBCO detectors. The work described above was completed at SMU without Raytheon participation.

II-1E. MAJOR ACTIVITIES IN TASK 3:

Electrical characteristics of pyroelectric modified lead titanate arrays were measured at different temperatures. These devices were fabricated at Raytheon Systems Company. Dielectric loss tangent ($\tan\delta$) as low as 0.045 at 30 Hz was obtained at room temperature with lanthanum nickel oxide electrodes. For the purpose of this study, micromachined 40×40-μm^2 pixels made of 200 nm thick pyroelectric films were connected in parallel into 10- or 100-pixel arrays. Noise measurements showed the temperature and frequency dependence of $\tan\delta$ noise to coincide with the calculated results. At room temperature, the best 10-pixel array showed a $\tan\delta$ noise current as low as 2×10^{-15} A/Hz$^{1/2}$ at the operating frame rate of 30 Hz. As expected, $1/f$ noise was observed proportional to applied current when the pixels were dc-biased. Details of the results are discussed in the Major Findings Section.

II-1F. MAJOR ACTIVITIES IN TASK 4:

Raytheon was successful in demonstrating thin film pyroelectric focal plane arrays using modified lead titanate detectors before its program was terminated and the group disbanded. The end of the Raytheon program made the cost of producing YBCO focal plane arrays prohibitive without the participation of Raytheon in this program. A side note, Mitsubishi recently reported on its independent (without any help from SMU) development of uncooled YBCO microbolometer focal plane arrays with an NETD of 70 mK. SMU has obtained funding from NASA to develop micro-pyroelectric detectors with on chip readout. At present, a scanned IR camera with external readout circuitry is being developed at SMU. The software for the camera is currently being refined in order to obtain imagery. The laboratory camera will allow imagery to be produced from the prototype detectors.

Dr. Celik-Butler and Dr. Butler have also received a grant from NASA to develop broadband FIR pyroelectric detectors with on-chip readout to continue this work. In this case, the CMOS readout circuit will be designed at SMU and fabricated at a foundry. The detectors will then be fabricated on the CMOS substrates at SMU.

REFERENCES

[1] B. M. Kulwicki, A. Amin, H.R. Beratan, and C.M. Hanson, *IEEE Symp. On Appl. of Ferroelectrics*, Aug. 1992.

[2] P.W. Kruse, *Infrared Phys. Technol.* Vol. 36, pp. 869-882, 1995.

II. ACTIVITIES AND FINDINGS

II-2 Major Research Findings:

II-2A. MAJOR FINDINGS FOR TASK 1 AND TASK 2:

Self-supporting IR Detector Structures:

Several different self-supporting structures were fabricated and tested. More than an order of magnitude of improvement was observed in responsivity, thermal conductance and thermal capacitance. The following Figures show the different self-standing structures designed, built and tested and the results obtained.

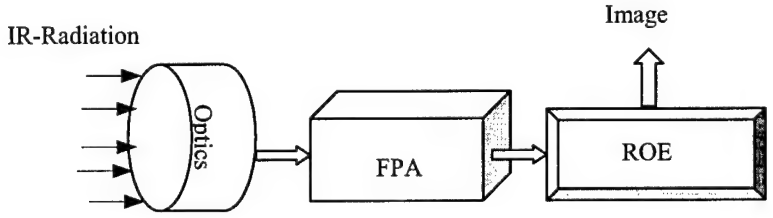

Figure 1. A block diagram of the infrared system. It consists of the optics, focal plane array, and the read out electronics and signal processing.

The devices MA1 and MA3 incorporated an Aluminum mirror under the pixel, and niobium arms. The devices MM1 and MM1 did not have a mirror under each pixel. However, a LaA_2O_3 layer covered the substrate to minimize any responses that might come from the substrate. The $LaAl_2O_3$ was chosen because it has low absorption of IR-radiation. The arms were titanium in these structures. Polyimide was used as a sacrificial layer for all self-standing microbolometers.

The general device fabrication for MA devices follows. A four-target, cryo-pumped, CVC601 sputter system was used for all depositions. Four-inch <111> Si wafers were thermally oxidized with 200 nm SiO_2. The aluminum (Al) mirror layer was deposited to be 100 nm thick by RF magnetron sputtering in 10 mTorr of Ar. The Al mirror was patterned by conventional photolithography and wet etching. The wafer was then coated with Dupont polyimide and soft baked for 40 min at 140°C. The polyimide was then cured at 300 °C in N_2 environment to obtain a durable film, 1.7 μm thick. The polyimide was then patterned into rectangular mesas using standard photolithography and etching with O_2 plasma. The Nb electrodes were deposited by RF magnetron sputtering. The nominal thickness of the Nb electrode was 170 nm. The Au contact layer was subsequently deposited without breaking vacuum. The Au layer was nominally 70 nm. The Au contact layer was subsequently deposited without breaking vacuum. The Au layer was nominally 70 nm thick. Dry etching with CF_4 patterned the Nb electrodes. A two-metal-electrode was employed since metals such as Au, pt, or Ag make the best electrical contact to Y-Ba-Cu-O. Nb makes a highly resistive contact to Y-Ba-Cu-O but is a relatively low thermal conductivity metal (0.219 W/cm K) and therefore provides better thermal isolation than if a single, high thermal conductivity metal such as Au (3.1 W/cm K), Pt (0.73 W/cm K), or Ag were used. Different contact sizes varying from 35×10 μm^2 to 10×10 μm^2 have been tried to explore the effects of contact size upon detector noise.

The YBaCuO thermometer layer was then deposited by rf magnetron sputtering at ambient temperature in 10 mTorr of Ar. The YBaCuO pixel was patterned using conventional photolithography and wet etching with a 1:20 dilution of Al-etch. The polyimide mesa was removed by ashing for 3-7 hours to suspend the YBaCuO pixel and form the thermal isolation structure.

The device geometry is shown schematically before and after etching the sacrificial layer along with scanning electron microscope micrographs in Figure 2.

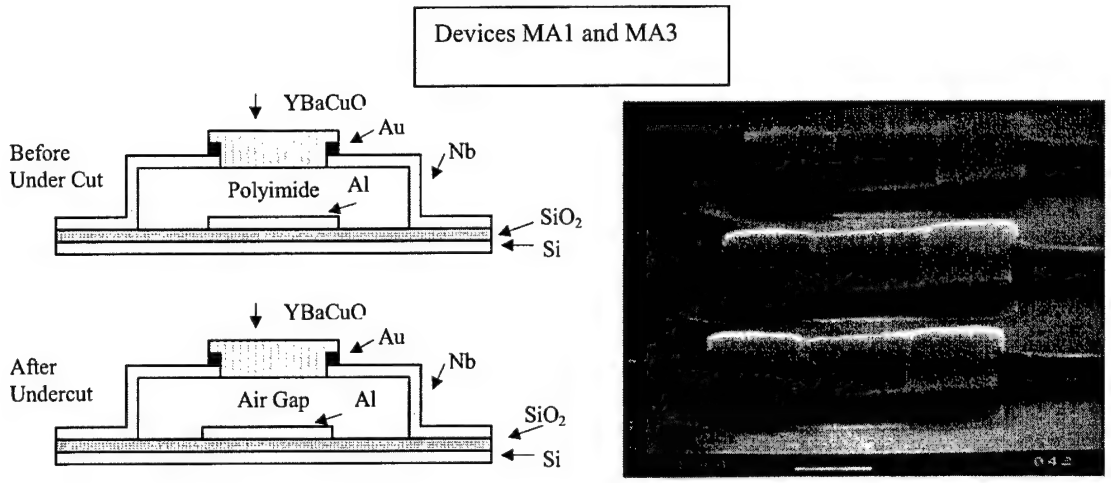

Figure 2. Self-supporting Y-Ba-Cu-O device geometry. 1×10 arrays were fabricated with 40 μm × 40 μm pixel size. Schematics of the process and SEM micrograph of the resulting devices are presented

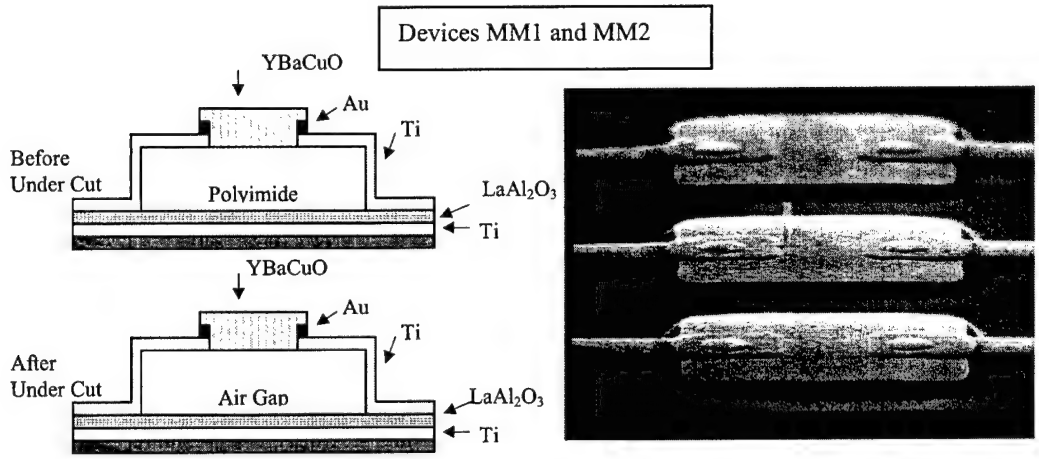

Figure3. Self-supporting Y-BaCu-O microbolometer geometry. 1×10 arrays were fabricated with 40 μm × 40 μm pixel size. Schematics of the process and SEM micrograph of the resulting devices are presented.

The general device fabrication for MM structures was slightly different. The <111> n-type 5-15 Ω.cm silicon wafer was covered by thick titanium metal layer deposited by RF magnetron sputtering at 150 watt in pure argon environment at 10-mTorr pressure. The nominal thickness of Ti was 300 nm. The titanium film was then exposed to O_2 by placing the wafer in a plasma etching system for 10 minutes. Metal was used in this first step to eliminate the substrate effect on the device in order to measure the real performance of the devices. Besides, thick titanium is a highly reflecting material. It reflects the IR radiation transmitted back to the pixel active area. Therefore, the sensing material Y-Ba-Cu-O will be exposed more to infrared radiation and it forms a resonant cavity structure to enhance the IR absorption.

Next, 300 nm of insulating material, $LaAl_2O_3$ was deposited by RF magnetron sputtering in pure argon environment at 100 watt. The $LaAl_2O_3$ was chosen because it has low absorption of IR-radiation. Next Ti mirror was deposited to be 100 nm thick by RF magnetron sputtering in 10 mTorr of argon. The Titanium mirror was patterned by conventional photolithography and dry etching techniques. The wafer

was then coated with Dupont polyimide (PI2610) and soft baked for 40 min at 140 °C. Next, the polyimide was cured at 300°C in N_2 environment to obtain a durable film, nominally 1.7 μm thick. The polyimide was then patterned into rectangular mesas using standard photolithography and etching with O_2.

Next, Titanium electrode and Au contact were deposited by RF magnetron sputtering, respectively. The nominal thickness of Ti electrode and Au contacts are 100 nm and 400 nm, respectively. Gold was patterned and Wet etched with KI-I_2 solution. Then titanium layer was patterned and dry was etched in a plasma reactive etching system (A24D). The semiconducting Y-Ba-Cu-O thermometer layer was then deposited by RF magnetron sputtering at ambient temperature in 10 mTorr of argon. The Y-Ba-Cu-O pixel was patterned using conventional photolithography and wet etching with 1:100 Al-etch. The nominal thickness was 400 nm. The polyimide mesa was then removed by ashing for 3-4 hours to suspend the Y-Ba-Cu-O pixel and form the thermal isolation structure. Figure 3 shows the MM structures.

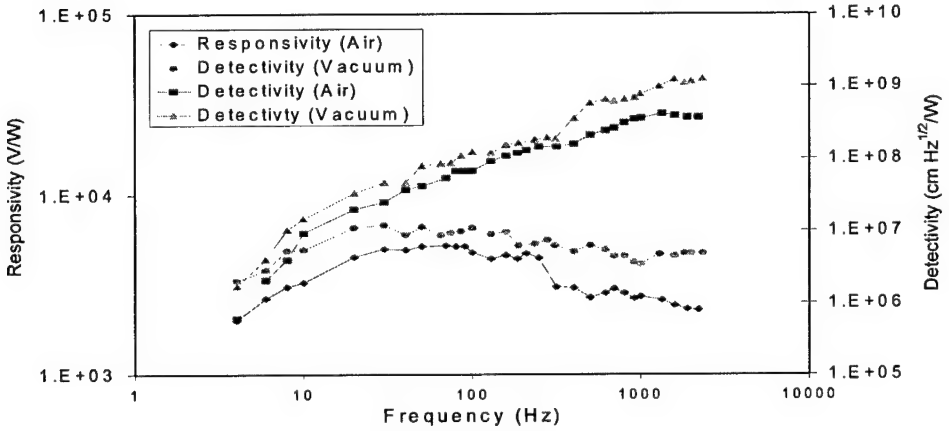

Figure 4. Zero-bias responsivity and detectivity of device MA3 measured as a function of chopping frequency

Table I. Summary of device properties for MA-type devices.

	Device MA1	Device (MA3)
YBaCuO thickness (nm)	400	400
Nb-electrode thickness(nm)	170	170
Au contact (nm)	70	70
Contact Area (μm)	10×35	10×10
2-wire resistance (MΩ)	3.5	2
TCR (%/K)	-3.5	-3.1
G_{th}(W/K)	2.9×10^{-6}	1.3×10^{-6}
Maximum Responsivity (V/W)	5268	6603
Maximum Detectivity (cm $Hz^{1/2}$/W)	2×10^{8}	1.1×10^{9}

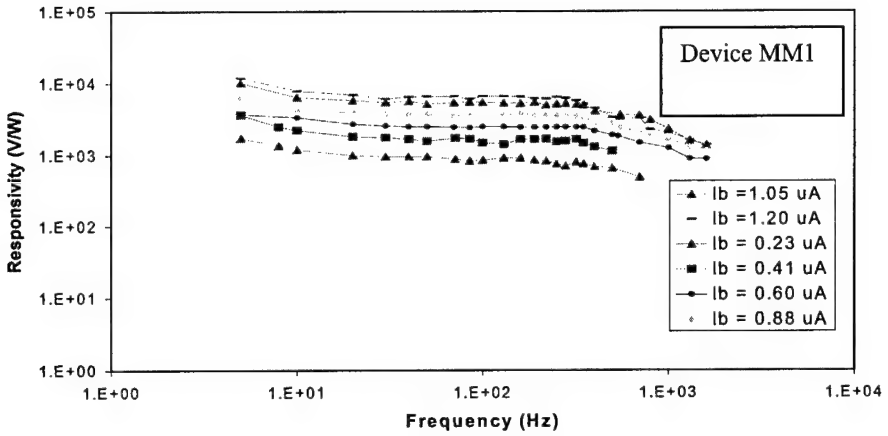

Figure 5. responsivity as a function of chopper frequency at different current biases measured in vacuum with 2.5 to 13 μm broad band IR radiation.

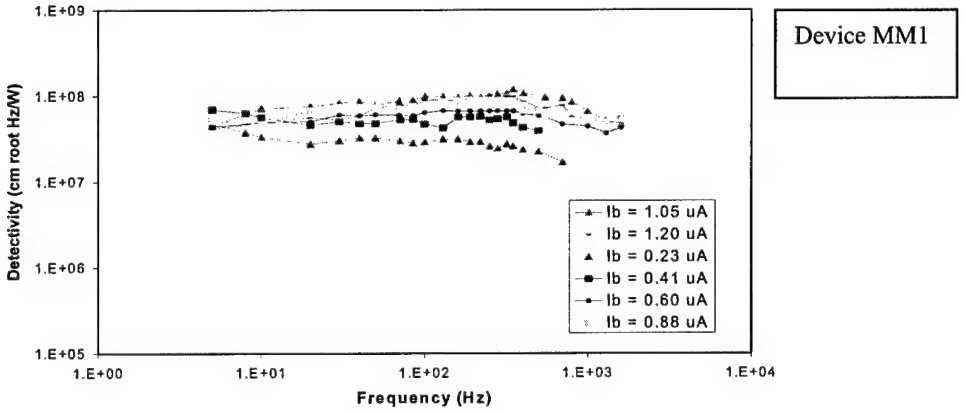

Figure 6. detectivity as a function of chopper frequency at different current biases measured in vacuum with 2.5 to 13 μm broad band IR radiation

Table II. Summary of microbolometer properties for MM-type devices.

	Device MM1	Device MM2
YBaCuO thickness (nm)	400	400
Ti-electrode thickness (nm)	100	100
Au contact thickness (nm)	40	40
Contact area (μm)	10×10	10×35
2- Wire resistance at 295 K (MΩ)	1	0.5
TCR (%K)	3.1	3
G_{th}(W/K)	1.9×10^{-6}	2.2×10^{-6}
Absorption η (%)	30	37
Thermal capacitance (J/K)	3.53×10^{-10}	4.2×10^{-10}
Thermal time, τ_{th} (ms)	0.17-0.22	~0.20
Maximum Responsivity (V/W)	7950 @ 1.05 μA	2011 @ 0.9 μA
Maximum detectivity (cm $Hz^{1/2}$/W)	1.185×10^{8} 1.05 μA	5.87×10^{7} @ 0.9 μA

High Absorptivity Resonant Detector Structures:

The performance of two different structures is presented here: namely, a micromachined bolometer and a detector with full contact to the substrate. Both structures employ an aluminum-reflecting layer under the bolometer. Micromachined devices were fabricated by depositing 3000 Å of YBCO thin film onto a 4000 Å SiO_2 bridge. In order to increase the absorptivity, a very thin layer of titanium was introduced on top of the sensitive area. An IR reflective layer of aluminum was used at the bottom of the cavity under the sensitive area. Opening trenches created the cavity after defining the sensitive region and removing the underlying sacrificial layer, which was a cured polyimide in this case, with a thickness of 1.7 μm to obtain maximum absorptivity at the sensor. The legs of electrodes were chosen to be titanium, providing a low thermal conductivity, while gold was used for contacts and pads as of being a highly conducting material and yielding low contact resistance to YBCO. The devices on silicon substrate were fabricated on a 8500 Å thick Si_3N_4 bridge with 4000 Å of YBCO. A passivation layer of 500 Å Si_3N_4 was introduced on top of YBCO followed by the same Ti absorption layer. The temperature dependence of resistance was measured between 220 and 310 K and Temperature Coefficient of Resistance (TCR=*(1/R)(dR/dT)*) was found to be –3.5% and –3.0% at room temperature for micromachined and non-micromachined devices, respectively. The responsivity of these devices showed a considerable difference due to the enhanced thermal isolation of the micromachined device. The thermal conductance to the substrate was found to change with ambient pressure for the micromachined device, while no such dependence was observed for the device on substrate. The micromachined detector yielded detectivity around 1×10^{7} cm $Hz^{1/2}$/W, while the latter showed a significantly lower detectivity of 2×10^{5} cm $Hz^{1/2}$/W.

The process for the micromachined pixel starts with the oxidation of <111> Si wafer using a wet oxidation technique at 1000 °C for 30 min, resulting in a SiO_2 layer with a thickness of 3000 Å. Thermally grown oxide isolates semiconducting Si from the device. All thin films were produced in an rf-sputtering system with a 3-inch target. Argon was used as a bombarding particle and during sputtering, pressure was kept at 10 mTorr in Ar background.

Aluminum was sputtered next onto the previously oxidized wafer producing a thickness of 1000 Å and then lithographically patterned and etched, coinciding with the IR sensitive area. The reflectance of Al in the wavelength region of 4-30 μm is above 0.980 but less than 0.995[1,2,3]. This thin Al layer at the bottom of the structure reflects the IR energy transmitted by the microbridge back to the bolometer active area, hence enhancing the absorption.

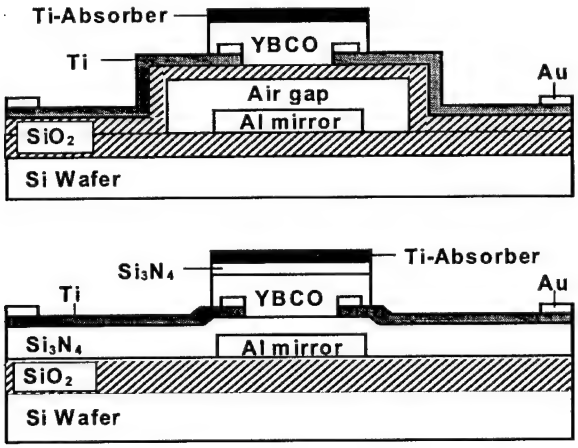

Figure 7: The cross-sectional view for (a) the micromachined bolometer (D1) and (b) bolometer on substrate (D2). (Not drawn to scale.)

The following step is to form a sacrificial layer using polyimide (PI2610). This is a good candidate with its relatively low dielectric constant, thermal stability and low moisture absorption for this specific design and application[4]. The thickness of the sacrificial layer was set to 1.7 μm by arranging the spinning and cure parameters. Having etched the polyimide with Al hard mask in the oxygen plasma etching system, SiO_2 film was sputtered to a thickness of 4000 Å to serve as a bridge material. A good feature of this oxide is its high transmittance in the IR region enabling the reflected IR energy from the Al mirror to be received by the active area. Another advantage is that the thermal conductivity of SiO_2 is lower than other common bridge materials such as Si_3N_4. The gap between the mirror and the bridge was designed to give maximum absorption over a perfect $\lambda/4$ cavity. Theoretically, nonspecular wavelength dependent diffusive and diffracted losses at the microbridge and the reflector layers should also be taken into account, but was neglected in this study. Therefore, a higher sensitivity is possible with a mirror under the pixel with a resonance gap of $\lambda/4$ left after the removal of the sacrificial layer.

Next a 900 Å of Ti was sputtered, followed by 800 Å of Au. Gold is easy to bond on but possesses a relatively high thermal conductivity of 3.18 W/cm K.[5] In addition, as an advantage, it forms a low resistance contact to YBCO. On the other hand, titanium provides a good electrical conductivity while having a relatively low thermal conductivity of 0.219 W/cm K.[5] These properties make gold a good material for contacts and pads and titanium for legs to prevent heat loss. In the fabrication process, gold was patterned and etched with a diluted solution composed of KI and I_2, leaving titanium metallization layer exposed. Then, titanium was patterned lithographically and dry-etched in a reactive plasma etching system in Ar and CF_4 ambient. The micromachined legs provide thermal isolation of the pixel. The legs should also be capable of providing structural support for the pixel while still maintaining low thermal conductance to the substrate.

The next step was to sputter the sensitive layer, the semiconducting YBCO, in Ar ambient at 10 mTorr. Approximately, 3000 Å of YBCO was deposited. The last deposition step was to sputter IR absorber layer, which was a very thin Ti layer in this case. Thin metal films are known to act as wide band absorbers for IR radiation with a very small heat capacity[6,7,8,9] The absorption is independent of the radiation wavelength as long as the radiation frequency is smaller than the reciprocal collision time of the electrons in the metal absorber layer. After the absorber layer and YBCO are lithographically patterned, they are etched with plasma etching and in a very dilute HCl solution, respectively. Having patterned the active area, pixels are ready to be released. For this purpose, the bridge material SiO_2 was trench patterned and etched with dilute HF solution, leaving openings to reach to the sacrificial layer. Polyimide is then etched with oxygen plasma with the same settings as before but for a longer time. This period of time depends on the curing process and the amount of surface exposed to oxygen bombardment. Introducing polyimide to the process has several advantages. Dry etch process has the advantage of a near zero etch rate of formerly deposited layers. It also allows the freedom to choose appropriate bridge material with desired thickness. At this point, the bolometer fabrication process was completed and devices were ready

for electrical bonding. Fig. 8 shows a SEM picture of a microbolometer structure. The cross-sectional schematic is depicted in Fig. 7(a).

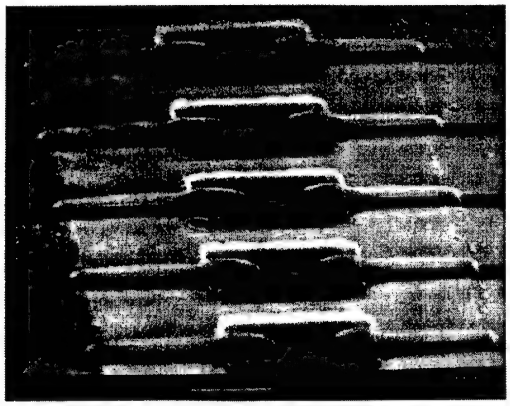

Figure 8: A partial SEM Micrograph of 1x10 bolometer array with 40x40 μm^2 dimensions.

The fabrication process for the detector on the substrate was very similar to that of the micromachined device. After having introduced the Al mirror layer onto thermally grown SiO_2, bridge layer of Si_3N_4 with a thickness of 8500 Å was sputtered. The same metallization process was used for the legs and the pads, followed by 4000 Å YBCO sputtering. The next step was to coat a passivation layer composed of 500 Å Si_3N_4 and the absorber layer. The top absorber layer was again composed of a very thin Ti layer. The next layer of Si_3N_4 was plasma etched in an ambient of Ar and CF_4, leaving YBCO exposed. Applying the same process as before, YBCO was patterned to define the sensitive area. The cross-sectional view of the bolometer on Si substrate is shown in Fig. 7(b).

The resistance versus temperature was measured on both structures. As expected, the temperature coefficient of resistance (TCR) was found to be around –3%. Responsivity of the micromachined bolometer was characterized using a chopped light from an Oriel 66337 IR source. Calibration was done with an Oriel 70124 pyroelectric detector. The light source was powered by a stabilized Oriel 68831 radiometric power supply. An AC coupled PAR113 preamplifier was used to amplify the signal and spectra were recorded with a HP3562A dynamic signal analyzer. The detector response was investigated at three different currents. The experiments were done in air and vacuum. Figs. 9(a) and 9(b) show the responsivity and detectivity of the micromachined pixel at different currents in vacuum and air. The outstanding difference between these two sets of measurements was the change in G value, namely, a decrease in the thermal conductance in vacuum yielding a higher responsivity and detectivity but a decrease in the roll off frequency. All sets of measurements were also repeated with a LP2500 filter and calibrated. The results showed that there was not any high-energy photon effect in the measurements. As expected, R_s showed a linear dependence on the bias current. The η/G values were calculated from $R_{s\text{-}max}$, at low frequencies through the expression for responsivity Using this η/G and G obtained from resistive heating method, absorptivity η was found out to be 29%. The time constant τ, was found from the best fit of responsivity equation to the experimental result, using corresponding I_b, α, R, G and derived η. The roll-off frequencies were 113 Hz and 318 Hz in vacuum and air, respectively.

The same characterization method was used for the bolometer on substrate. The two-probe resistance values varied from 0.3 to 2 MΩ with geometry. The bolometer tested had a dc resistance value of 0.430 MΩ at room temperature. The reason for the relatively low resistance is the thicker YBCO film. Two-probe R-T measurement from 220 to 320 K yielded a TCR of –3.0 %. The thermal conductance was found by joule heating method to be 3.98×10^{-4} W/K. The relatively high value of G is simply due to the thermal heat loss through the substrate. This leads to a higher roll-off frequency in responsivity curve, which scales as $1/\sqrt{\omega}$.[10] The responsivity measurements were performed at three different current biases resulting in the same voltage as the micromachined device.

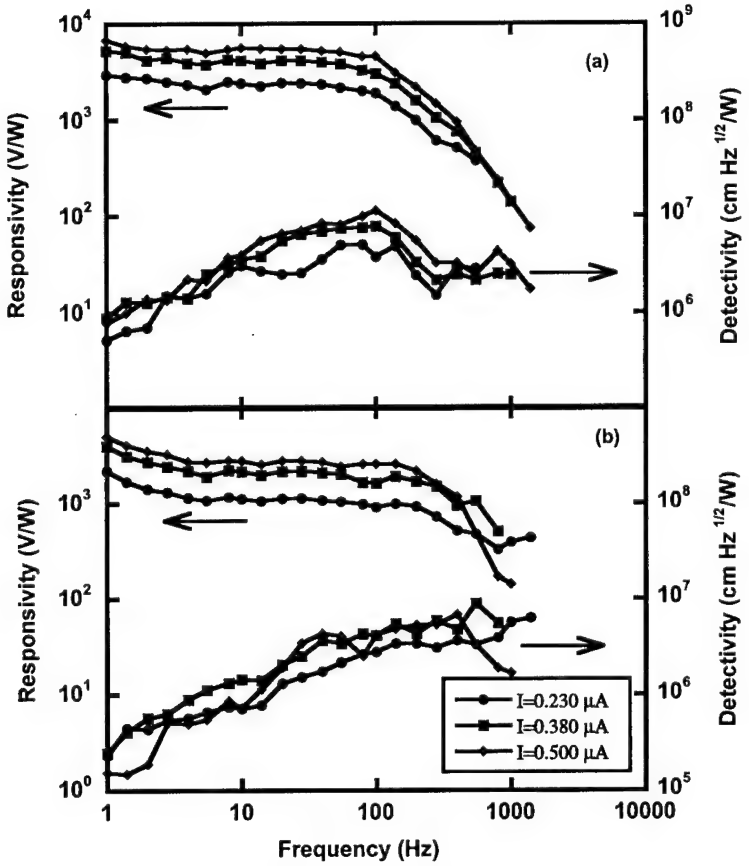

Figure 9: Responsivity and detectivity of the microbolometer (D1) at three different current biases versus chopper frequency, (a) in vacuum, (b) in air.

A summary of measured and derived parameters for five different IR detectors is shown in Table III. Detector 1 (D1) is the micromachined bolometer and Detector 2 (D2) is the one with full contact to the substrate. Detector 3 (D3)[11] is another micromachined bolometer with 2000 Å YBCO deposited on a 15000 Å SiO_2 layer as the bridge material. Detector 4 (D4)[12] is basically similar to D3 except a different contact point configuration. Detector 5 (D5)[13] has a 1000 Å YBCO on a 4000 Å thick Si_3N_4 bridge. Detectors 3 to 5 have been reported before and included here merely for comparison.

In addition to the different IR sensitive region thicknesses and the bridge structure, these bolometers have different contact sizes and locations on the pixel. Contact areas differ from 10 x 10 μm^2 to 60 x 25 μm^2 (drawn dimensions). These contacts are located either across each other (I structure) or at the diagonal corners (Z structure) of the pixel. The contacts play a major role in the overall pixel resistance and should provide an Ohmic contact. Contact material is the same, namely, Au in each device, whereas the electrode material is different as shown in Table III. Gold does not have good adhesion to most materials but to Ti and its response to ultrasonic wire bonding is good as long as it is thicker than several hundred angstroms. The other alternative for gold would be silver. For the micromachined bolometers, electrodes are usually the most significant component of heat conduction. Hence, the lower the heat conductivity, the better the responsivity. In terms of heat conductivity of the metals, Ti has the lowest value while Nb has 2.3 times higher than that of Ti. Gold has a relatively high value for this parameter and a bad candidate for the electrodes.

The discrepancies among the resistance values of similar devices are due to the size of contacts, namely, point and large area contacts or to arm length of the electrodes. The differences between the

resistance of different structures basically stem from the change in the thickness or stoichiometric variations such as oxygen content of YBCO thin film. Nevertheless, high resistance is not a significant problem because responsivity linearly depends on resistance. On the other hand, higher resistance means a higher Johnson noise floor, which comes into consideration for detectivity calculations. The slight variation of TCR values can be explained by different deposition conditions resulting in a change in the composition of the sensitive film and therefore, activation energy for conduction.

Table III: Comparison of different semiconducting YBCO-based bolometers. The subscript *th* refers to the calculated values for thermal conductance and thermal capacitance using the thermal conductivity and the specific heat of the materials used in the structures.

	D1	***D2***	***D3 (ref.11)***	***D4 (ref. 12)***	***D5 (ref. 13)***
YBCO Thickness (Å)	3000	4000	2000	2000	1000
Size (μmxμm)	40 x 40 (I)	60 x 60 (I)	40 x 40 (I)	40 x 40 (Z)	40 x 40 (Z)
Contact size (μmxμm)	6 x 6	54 x 23	10 x 10	10 x 10	35 x 10
***R* range (MΩ) (depending upon geometry)**	2 - 9	0.3 - 2	2 – 10	2 - 10	3 - 7
***TCR* (%) at 295 K**	3.5	3	3.4	3.25	2.8
Bridge Material [Thickness (Å)]	SiO_2 (4000)	Si_3N_4 (8500)	SiO_2 (15k)-MgO (400)	SiO_2 (15k)-MgO (400)	Si_3N_4 (4000)
Electrode Material [Thickness (Å)]	Ti (900)	Ti (900)	Au (2000)	Au (2000)	Nb (300)
$R_{s\text{-}max}$ **(V/W)**	5.6×10^{3} at 0.5 μA	2.04×10^{1} at 8.41 μA	1.43×10^{4} at 1.5 μA	8×10^{3} at 0.79 μA	6×10^{4} at 0.79 μA
D_{max} **(cm Hz$^{1/2}$/W)**	1×10^{7}	2×10^{5}	9.45×10^{7}	2×10^{7}	1×10^{8}
***G* (W/K)**	7.60×10^{-6}	3.98×10^{-4}	8×10^{-6}	7.41×10^{-6}	5.70×10^{-7}
G_{th} **(W/K)**	1.69×10^{-6}	8.10×10^{-3}	1.69×10^{-5}	1.69×10^{-5}	9.92×10^{-7}
η **%**	29	7.8	25-27	29	29
τ **(ms)**	1.4	<0.14	0.53 – 0.58	0.7-1.4	6
τ_{th} **(ms)**	1.4	7.06×10^{-3}	0.56	0.56	1.4
***C* (J/K)**	1.06×10^{-8}	$<5.57\times10^{-8}$	$4.2\text{-}4.6\times10^{-9}$	1×10^{-8}	$3.8\ 10^{-9}$
C_{th} **(J/K)**	2.34×10^{-9}	5.72×10^{-8}	9.56×10^{-9}	9.56×10^{-9}	1.38×10^{-9}

The thermal conductivity of the micromachined devices is mainly determined by the metal electrode arms, except for D5, which possesses a very thin layer (300 Å) of Nb as the metal electrode arms. For D1 and D2, Ti was used for electrodes while Au was the electrode material for D3 and D4. The

electrode thickness is 900 Å for the first two, 2000 Å for the following two and 300 Å for the last one. Having given these values, the other crucial component for G, namely the bridge material should also be mentioned. D1 possesses a 4000-Å SiO_2 bridge material similar to detectors D3 and D4 except with a thickness of 15000 Å. D2 is built on 8500 Å Si_3N_4 but the following layers also play a role in G of this device since it rests fully on the substrate. Therefore, radial heat transfer into the substrate was also considered in calculating G, but the Kapitza thermal resistance between the layers was neglected, which might account for the discrepancy between the measured G and the calculated G_{th}. D5 possesses a 4000-Å Si_3N_4 bridge material, which contributes equally to the total thermal conductance as the Nb arms. Among the detectors listed in Table III, the lowest G value is obtained on D5. This could be due to very thin electrodes, which are only 300 Å thick Nb films. The high G value for D3 and D4 are basically due to the domination of Au electrodes with a 14.5 times higher thermal conductivity than that of Ti. Although SiO_2 is an advantage with a relatively low thermal conductivity for the micromachined device described in this article, the overall G value for this device is still high since Ti contribution dominates.

Heat capacity of the detectors is mainly determined by the YBCO film, bridge material and the electrodes. D5 has the smallest C value because the specific heat capacity of Si_3N_4 is 3.9 times smaller that of SiO_2 and of the thin film YBCO. G and C are the factors, which determine the time constant τ, consequently the roll-off frequency. Since C is not a function of ambient pressure but G is, the shift at the corner frequency to the lower values in vacuum due to a decrease in G should be expected. However, for the device on substrate, G is relatively high and is dominated by the substrate. Hence, a shift in the roll-off frequency was not observed for the device on substrate when the ambient pressure is increased. For D1, while G was $7.6\text{x}10^{-6}$ W/K in vacuum, this value increased to $1.59\text{x}10^{-5}$ W/K in air, which resulted in the observed shift of roll–off frequency to lower values in Fig. 9. The heat conductivity in air was derived by comparing responsivity measured in air and vacuum, and assuming that the absorptivity η remains the same.

Even though D1 had a Ti absorber, η is about the same as D4, and D5, which do not have an absorber. Absorptivity of D2 is small due to the lack of resonance cavity. It seems that the cavity under the pixel and the aluminum mirror layer play more important role in enhancing the absorptivity than the Ti layer. These values are not direct measurements but derived from $R_{s\text{-}max}$ and G values. For more precise measurements, optical techniques should be used[14].

As expected, responsivity scales with bias current. D5 with the smallest G has the highest $R_{s\text{-}max}$ value, considering the direct proportionality of the current bias as well. D1, D3, and D4 have very close $R_{s\text{-}max}$ values if normalized by the bias current. This is an expected result because these detectors have similar G values. Since G of D2 is relatively high, $R_{s\text{-}max}$ of this device is expectedly low.

The major limiting factor for the detectivity is the noise. The detectivity is usually limited by Johnson noise at higher frequencies and by *1/f* noise at low frequencies. The measured detectivity of $1.12\text{x}10^{7}$ cm $Hz^{1/2}/W$ is close to the Johnson noise limited detectivity of $5\text{x}10^{7}$ cm $Hz^{1/2}/W$ possible for the measured responsivity. However, at low frequencies, these devices possessed an unusually high level of 1/f noise.

Laser Annealing of YBCO Thin Films

The structural [15,16], electrical [15,17,18], and optical [15,19] properties of $YBa_2Cu_3O_{6+x}$ can be varied by adjusting the oxygen content x. $YBa_2Cu_3O_{6+x}$, referred to as YBCO from here on, changing from an insulator ($x \approx 0$) with a tetragonal crystal structure to a semiconducting Fermi glass for $x \approx 0.3\text{-}0.5$, and then to a superconductor with an orthorhombic crystal structure as the oxygen molar content approaches 7. We can conclude that it is the oxygen content, which is the most critical in determining the phase of this material and its transport characteristics [20]. In addition, by adjusting the oxygen content, the same material can function as a pyroelectric detector when fabricated in a capacitor structure [21], [22] [23], exhibiting typical perovskite characteristics.

This investigation describes a study of higher TCR and resistance measurement for YBCO by changing its oxygen content. Here, post-deposition pulsed laser annealing (PLA) procedure was used change the oxygen content of the samples. Electrical characteristics were measured to evaluate the optimum oxygen content under which this material would function as a better bolometric material for IR radiation detection around room temperature. Various samples were prepared using different annealing

conditions (varying laser power and number of pulses) and compared to each other to find the best one as an IR sensitive detector material.

Pyroelectric devices were prepared with annealed sensitive material (2,000Å YBCO) to observe changes in loss tangent. Loss tangent was calculated from experimentally measured capacitance and resistance of the device. A frequency range from 20 to 1000 Hz was scanned. The same measurements were repeated at different temperatures in order to observe changes in loss tangent with respect to temperature.

For the annealing procedure, excimer laser was used. Laser annealing is a technique that is becoming increasingly popular in microelectronic fabrication. One important application is Si on insulator devices. Excimer lasers have been used to convert amorphous Si to Poly-Si for the fabrication of thin film transistors for flat panel displays [24], [25]. Additionally, excimer lasers have been used to anneal SiN_x films [26], Pd/SiGe contacts [27], and n-GaAs contacts [28].

Pulsed annealing has a number of advantages compared to constant annealing. Namely, it is easy to reach high temperatures in a fraction of a second and to localize the region of heating. This provides annealing circumstances suitable for forming new phases around non-equilibrium concentrations of the point defects. However, depending on the pulse duration, the substrate material and cooling rate during pulsed laser treatment, the treated films and metal-semiconductor systems are characterized by the formation of zones with non-equilibrium defects, clusters and pores which highly affect the electro-physical parameters of thin-film materials. Earlier researches have shown that illumination of high temperature superconductor samples allows them not only to investigate the electron states in various ranges of energy but also to modify their properties dynamically [29]. Generation of non-equilibrium charge carriers, in specific circumstances (atmospheric or some specific gas environment), increases conductivity and enhances superconductivity in metallic samples [30]. Furthermore, some researchers used excimer laser annealing technique to obtain high-performance, low-temperature poly-silicon thin-film transistors (TFT's) from amorphous-silicon without causing any damage to the glass substrate [31]. Additionally, some studies on laser annealing of lead titanate have already been conducted to obtain not only crystallization, but also good ferroelectric properties by laser annealing after constant annealing at temperatures 475-550 °C [32].

Typically our samples are amorphous when they are deposited by RF sputtering. X-Ray diffraction patterns of samples were taken before and after annealing to investigate the degree of crystallization. The oxygen content as well as the range of crystallization was varied by pulsed laser annealing. We have not performed any composition study on the samples. Hence, change in oxygen content was concluded from change in resistance. The figures of merit for IR detection were measured on each sample. A variety of annealed samples were prepared and compared to each other to find the best one as a detector sensitive material.

Fabrication process begins with 2,000 Å oxidation on <111> n-type Si, which electrically isolates the sample layer from the wafer. Sample material, 2,000 Å YBCO, is deposited by RF magnetron sputtering from a 3-inch diameter target at 90 W power. Material layer is deposited at ambient temperature in order to maintain compatibility with the CMOS technology. During deposition, pure argon is used and pressure is kept at 10^{-2} mmHg.

Using excimer laser ($\lambda = 248$ nm), samples are annealed under vacuum ($\sim 10^{-5}$ mmHg) to decrease the oxygen content. When ultraviolet light hits the surface of sample, it will absorb light because laser has a short wavelength. After absorption, temperature of the sample increases and some bonds are broken. Thus, some oxygen atoms will be released. These oxygen atoms can be taken away from the sample under high vacuum.

Annealing proceeded at various power and pulses (laser shots) at 1 Hz frequency to obtain samples with different oxygen content and range of atomic order. We investigated 20 and 25 mJ/cm^2 power and 100, 200, and 300 pulses for each power.

The output of the excimer laser resembles a Gaussian function on horizontal direction and is uniform on the vertical direction. To get a uniform illumination on the horizontal direction, we used a concave lens to enlarge the laser beam. Additional optics was also used to obtain different levels of power and to control the illumination area.

After annealing, the samples were pasted to ceramic packages using silver colloidal paint. Lastly, electrical connections were made to samples using an ultrasonic bonder to prepare them for measurements.

The variation in resistance with temperature was measured by mounting the sample in a Leybold ROK-300K closed-cycle cryostat evacuated to 5×10^{-2} mmHg, while the current was supplied by a Hewlett-Packard 34401A Multimeter in resistance measurement mode. TCR was calculated from Resistance-Temperature (*R-T*) curve. Our main interest was in the range of 230 K to 300 K. Four-point probe measurement technique was used to measure the resistance, using a constant current source.

TCR was calculated from the *R-T* curves. In semiconductors, resistance is an exponential function of temperature. Therefore, 5 points (two on each side of the point of interest) were chosen to match a best-fit exponential curve for experimental *R-T* curve.

The resistances of normal and annealed samples are compared in Fig. 10(a). The annealing power was kept constant to examine the change with pulse-number. It can be seen that with 100 pulses, there is a small increase in resistance. But with 200 pulses, a significant increase can be observed. That implies that the oxygen content of the sample is starting to decrease. With 300 pulses, we observed a reverse trend, a decrease in resistance compared to the 200-pulse sample. From Fig. 10(b), a slight increase in TCR magnitude can be noticed with 100-pulses. But with 200-pulses, TCR shows a considerable increase in magnitude. However, with 300 pulses, TCR slightly decreases in magnitude. It can be concluded that there is a threshold for annealing for pulse-number to cause an increase in resistance and TCR. In addition, some level of reversal occurs after 300 pulses, where the resistance starts to decrease.

In order to examine the level of crystallization in annealed samples, X-Ray diffraction patterns were taken on the samples. Fig. 11 shows XRD patterns taken for amorphous (normal) and annealed (power = 25mJ/cm^2, pulse = 300) YBCO respectively. Both films were sputtered as 2000 Å thick on oxidized Si n-type <100> wafers. Copper $K\alpha$ radiation, which has a wavelength λ of 1.54 Å corresponding to 8.048 keV, was used.

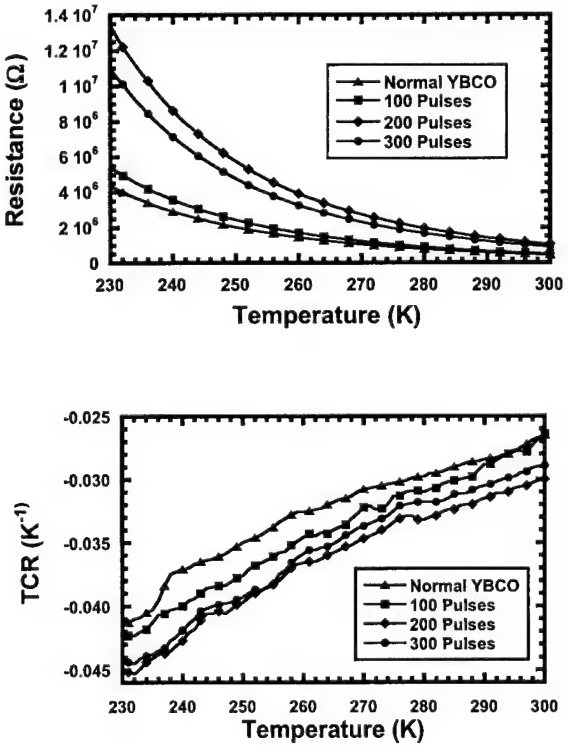

Figure 10 (a) Resistance and (b) TCR curves for normal (amorphous) and annealed YBCO. Laser power is 20 mJ/cm^2.

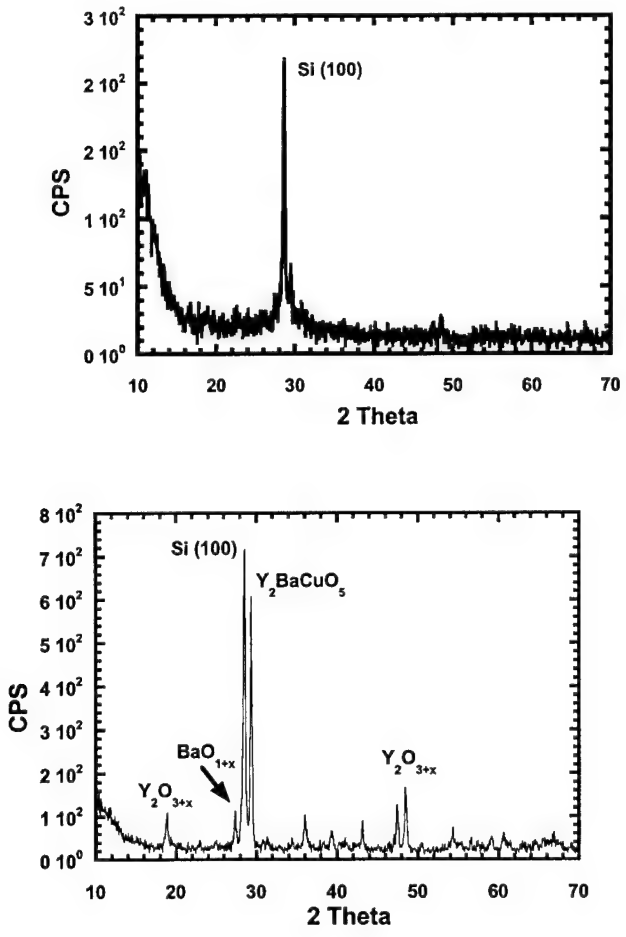

Figure 11 X-Ray Diffraction patterns of (a) normal (amorphous) and (b) laser annealed YBCO (power= 25 mJ/cm^2, pulse number = 200).

The study of the film microstructure using XRD reveals that the films are predominantly in an amorphous state as-deposited and progressively transform into a crystalline form with annealing treatments. An amorphous film lacks the regular arrangement of atoms required to form a crystalline structure and its resulting XRD scan would show no apparent peaks. The near absence of XRD peaks other than those from the underlying Si(100) substrate can be seen in Fig.11(a). As films crystallize during annealing treatments, they start to exhibit strong XRD peaks, as evidenced in Fig.11(b). A close examination of these XRD peaks indicates that the annealed microstructure does not consist of one phase but includes several sub-phases of YBCO. Due to the complexity of the film microstructure after annealing, the exact identity of the major phase and sub-phases are currently not clear. The complexity of the film structure appears to stem from the unique phase transformation process involved in laser annealing. In this process, the oxygen out-diffusion and crystallization concurrently occur, both of which should initiate at the surface and move deeper into the film. It is, therefore, likely that the kinetic interference between these two competing processes yields an inhomogeneous distribution of constituents, and thus, phases, forming throughout the thickness of the film. The same effect may also play a role in distorting the crystal structure of phases from their equilibrium states.

No direct measurement has been performed on samples to find out the composition and phase before or after annealing. However, considering all possibilities of phase formations and crystal

structures, an effort is made to identify the phases present in the annealed film from XRD pattern peaks. While other possibilities do exist, it is most likely that the predominant phase in the film is close to Y_2BaCuO_5. The possible sub-phases present in the films are determined to be Y_2O_{3+x} and BaO_{1+x}. Although the phase formation is complex and inconclusive, XRD results in conjunction with the characterization of electrical properties do suggest that crystallization by laser annealing produces phases that enhance the electrical properties of the films.

To investigate the effect of laser annealing on the pyroelectric properties, a 2,000 Å layer of SiO_2 was grown by wet oxidation technique on <111> n-type Si wafers to obtain an isolation layer. Subsequently, a 3000 Å Nb and a 2000 Å YBCO were sputtered, both at room temperature. The wafers were annealed using PLA. Different parts of the wafer were illuminated with different power levels and pulse-number. Another 3,000 Å Nb film was deposited onto the annealed YBCO. All sputtering processes were performed at 10^{-2} mmHg Ar. The Nb was plasma-etched to define the top electrode surface of the device while YBCO was wet-etched with a 16:1:1:2 solution of H_3PO_4:HNO_3:CH_3COOH:H_2O. Each capacitor had an effective area of 7.35×10^{-4} cm^2 in contact with the substrate.

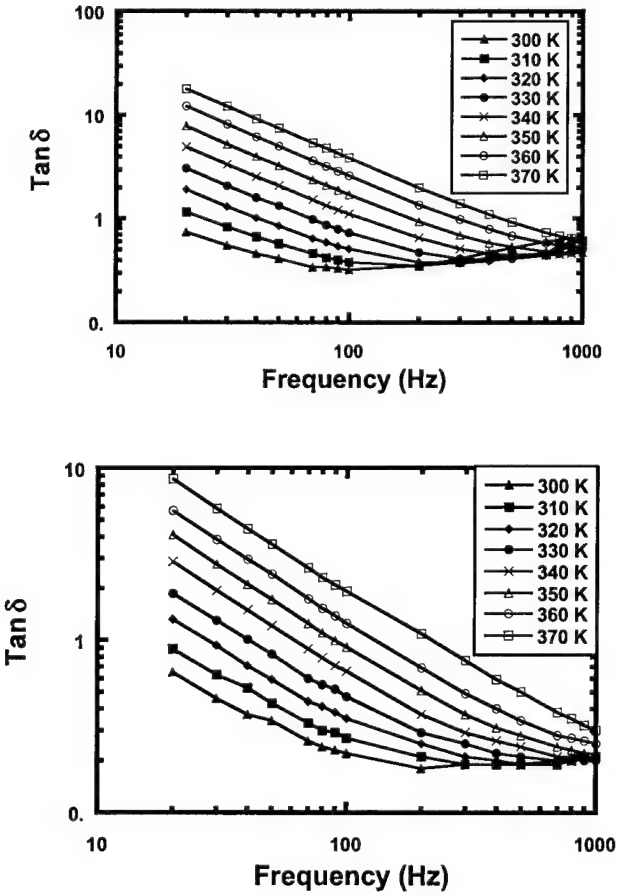

Figure 12 Loss tangent of annealed YBCO at different temperatures (a) power = 25mJ/cm^2, pulse number = 50 (b) power = 40 mJ/cm^2, pulse number = 50.

After the fabrication, the wafers were diced, packaged and bonded. The packages were mounted in a closed cycle refrigerator controlled by a LakeShore model DRC-91C temperature controller to take measurements at various temperatures. Pressure was kept at 5×10^{-2} mmHg. The capacitance and the resistance of the devices were measured with an HP 4284A Precision LCR Meter from 20 to 1,000 Hz

frequency range. Frequencies below 20 Hz were not measured due to high error associated with the increased parasitic capacitive effect at these frequencies.

The loss tangent data of annealed samples at different temperatures are plotted as a function of frequency in Fig. 12. We can observe an increase in loss tangent with increasing temperature. Another sample with higher (40mJ/cm^2) and the same pulse number (50) was prepared to investigate any change with power. We obtained 14% and 50% less loss tangent at room temperature and 370 K, respectively. We also took data on another sample with the same power (40 mJ/cm^2) and double pulse-number (100) in order to compare changes with respect to pulse-number. No considerable change, however, was observed in loss tangent.

It should be noted that study of loss tangent on amorphous to polycrystalline YBCO was reported before by Gray et al. [33]. Although the values measured here are higher than the ones reported by Gray, the same dielectric relaxation behavior can be observed for the same frequency range as shown in Figure 12. In [33], it was suggested that the dominant permittivity mechanism originated from the localized holes near the Fermi level. For a good pyroelectric IR detector, the loss tangent should be several orders of magnitude lower than the values reported here.

Pulsed laser technique offers a potential effective way of annealing infrared detector arrays with minimal damage to the underlying electronics. Thermal budget problem is an important issue for the deposition of ferroelectric thin films. Often, thin films are deposited by pulsed laser deposition (PLD) technique at substrate temperatures 700 °C or greater. Laser annealing has been used on a variety of systems over past twenty years. It has been demonstrated that thin films and surfaces can be heated to high temperatures without affecting the underlying bulk material. This technique is attractive to devices employing polyimide sacrificial layers. The previous work on ferroelectric thin films conducted by others has demonstrated that good pyroelectric properties can be obtained through laser annealing [32]. Our work has demonstrated that oxygen content of YBCO can be changed to get higher TCR and resistance leading low loss tangent values. Moreover, we have observed different crystallization levels for different annealing conditions. Both laser power and number of pulses determines the resistance of the annealed sample. The loss tangent, however, was found to be affected more strongly by the laser power. This implies that the dielectric constant is also affected by laser annealing.

Higher TCR was observed for good IR radiation performance in laser-annealed samples. We reached 3% TCR at room temperature with annealing process, which is more than 12% improvement. It can be concluded that detector responsivity will increase at least by 12%. Since annealing increases resistance of the detector as well, it will proportionally contribute to the responsivity.

Lower loss tangent was observed in pyroelectric devices with increasing power level. Only slight changes were also observed with increasing pulse-number. The maximum effect in loss tangent (50% decrease) at high temperatures (~370 K) was detected. However, this change dropped to 14% at room temperature. The crystallization of YBCO with annealing was confirmed with XRD measurements.

Broadband Detector Structures with Dual Resonant Cavities

The work reported here extends the wavelengths detected to 0.6 to 100μm with much larger detector size, up to 1.5x1.5 mm^2. These microbolometers are fabricated with a conventional polyimide sacrificial layer to further demonstrate the compatibility of YBaCuO thermometers with post-CMOS micromachining technology.

The noise voltage, ΔV_n, includes the background noise produced by the blackbody emissions of the surroundings, the temperature fluctuation noise due the fluctuation in the heat exchange between the isolated sensor and its heat sink, and the noise generated by the thermometer. The thermometer noise is made up of Johnson noise and 1/f-noise. Hence, for good performance, a microbolometer must have large values of β, R_V, and D^*. The noise corner frequency f_c is the frequency, at which the 1/f-noise merges with the Johnson noise,

$$\frac{\Delta V_n^2}{\Delta f} = \frac{\alpha_H I_b^2 R^2}{f_c N} = 4kTR \qquad (1)$$

The power-normalized 1/f noise corner frequency is used to make quantitative comparison between microbolometer devices. Here, α_H is Hooge's noise coefficient, N is the number of fluctuators in the sample, k is the Boltzmann constant and T is the temperature.

$$\frac{f_c}{I_b^2 R} = \frac{\alpha_H}{4kTN} = \frac{1}{4kT}\left(\frac{\Delta V_n}{I_b R}\right)^2 \frac{f}{\Delta f} \qquad (2)$$

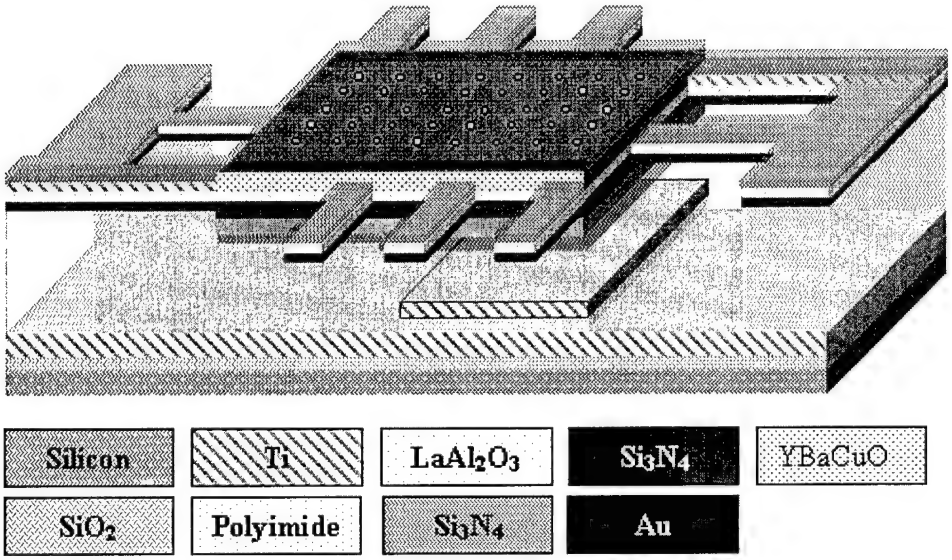

Figure 13. The 3-D view of room temperature broadband microbolometer geometry. The schematics show the device geometry consisting of double mirrors, double absorbers, Si_3N_4 membrane and passivation layer, and Ti electrode arms with Au contacts to the YBaCuO thermometer.

In design, a novel two-micromirror structure was used to achieve a relatively flat spectral response compared to a single microcavity design. To achieve a relatively flat spectral response, the thickness of the bolometer bridge, the thickness of the Ti absorber, and the height of the two air gaps between the suspended thermometer and the underlying mirror were designed to created an area-weighted impedance match between the detector and free space. The result was a flattened spectral response when compared to a single resonant cavity design. In this case, the areas of the two mirrors forming the two microcavities were set to be equal and the cavity heights and thickness of the thin films comprising the suspended bridge were optimized to provide the flattest possible spectral response using estimated optical properties for the constituent materials. The net effect was to use two ¼-wave resonances to minimize the fluctuation in the spectral response and achieve the desired broadband impedance match. A 3-D view of the 400×400-μm^2 microbolometer is shown in Figure 13. For a single mirror, the absorption varies from its maximum to the minimum. The absorption spectra for a single-mirror microbolometer is calculated using a combination of measured and published data for the materials of the single-mirror structure in a transmission-line model. The results are plotted in Figure 14. It should be noted that a regular resonance pattern is not observed because the YBaCuO and Si_3N_4 films also provide resonance that is mixed with the resonant behavior of the cavity. The resonance within the YBaCuO and Si_3N_4 films occurs at shorter wavelengths due to their approximately 400-nm thickness.

In the two-mirror structure, two mirrors with equal areas are employed under the pixel with two absorbers. In this case, one mirror is roughly tuned towards absorption at longer wavelengths, while the second mirror is tuned towards mid-wavelengths with cavity heights of approximately 2.73 μm and 3.68-μm respectively. The two absorbers have different thickness to account for the increase in the conductivity of the metal (Ti) at longer wavelengths. The values for different layer thickness and mirror heights were obtained by optimizing the absorption to provide a relatively flat spectral response over the spectral band of 0.3 μm to 100 μm.

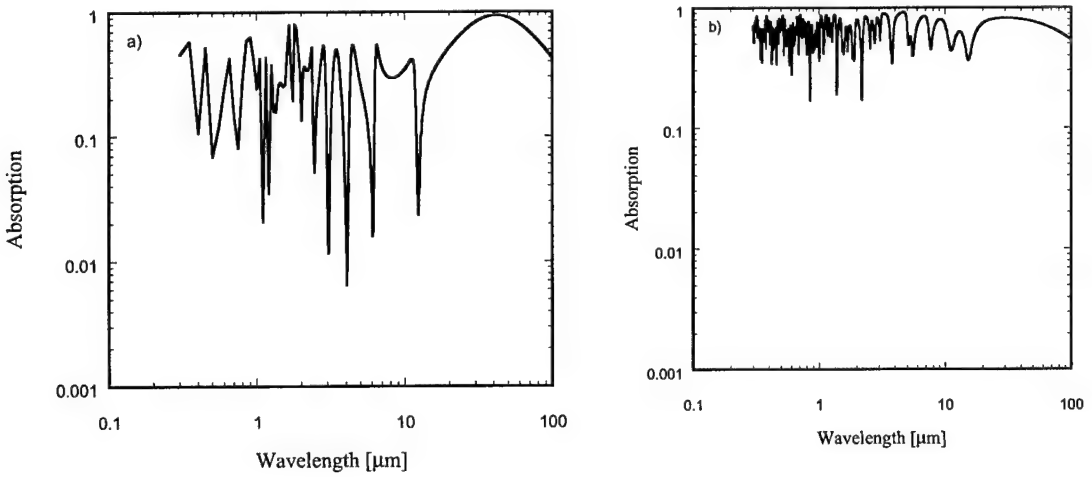

Figure 14. Calculated absorption spectra for a) one-mirror b) two-mirror microbolometer designs. The two-mirror design considerably flattens the spectral response of the microbolometer.

The YBaCuO microbolometers reported in this paper were fabricated using conventional polyimide sacrificial layers and a Si_3N_4 supporting membrane. An SEM micrograph of the resulting devices is shown in Figure 15. The general device fabrication procedure follows. A four-target, cryo-pumped, CVC601 sputter system was used for all depositions. A 300-nm thick SiO_2 was thermally grown on <111> p-type silicon wafer for insulation. Then, a thick Ti metal mirror was deposited by RF magnetron sputtering at 150 watt in 10 mTorr of pure argon environment. The nominal thickness of Ti was 370 nm. The continuous Ti mirror prevents the excitation of the electron-hole pairs in the substrate. In addition, it reflects the IR radiation transmitted back to the active pixel area, forming a resonant cavity with the YBaCuO thermometer to enhance the IR absorption. Next, the wafer was coated with a polyimide and soft baked. The polyimide was subsequently cured at 270°C in N_2 environment to obtain a durable film, nominally 2.33 μm thick.

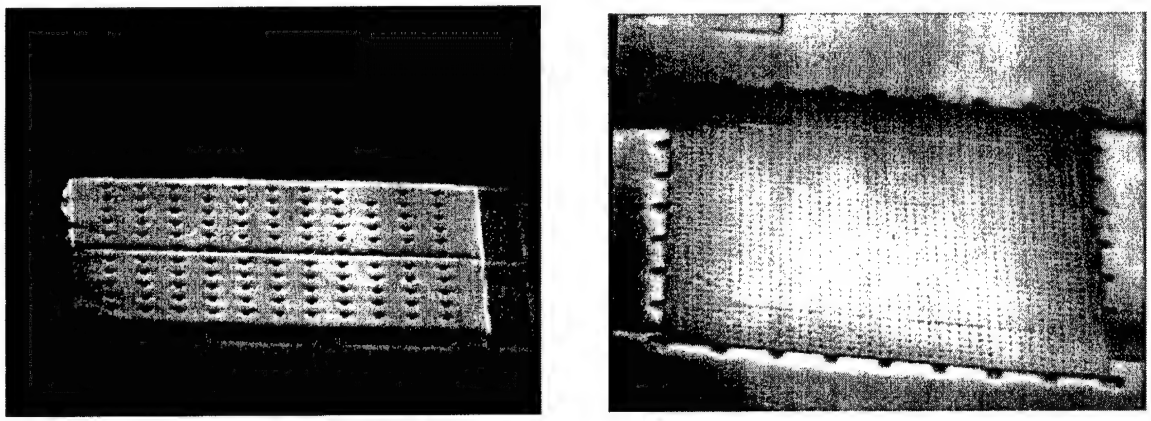

Figure 15. An SEM micrograph of the resulting devices. One 400μm ×400 μm^2 pixel from a 1×4 array is shown on the left. The array is diagonal. The photo on the right shows a single pixel with 1.5 × 1.5 mm^2 size.

The second 300-nm thick Ti mirror was similarly deposited by RF magnetron sputtering and patterned by conventional photolithography. The second polyimide sacrificial layer was then spin-coated and cured to the nominal thickness of 3.68 μm. A thin Si_3N_4 passivation layer was subsequently deposited followed by a sputtering of a thin titanium absorber. The passivation and absorber layers were then patterned and wet-etched. These thin films have the same area as the pixel. The thickness of the passivation and Ti-absorber were 12.8 nm

and 4 nm, respectively. Next, 236.7 nm thick Si_3N_4 membrane material was deposited followed by 23.3 nm of $LaAl_2O_3$. This layer is used as an etch stop to protect Si_3N_4 during plasma etching Ti electrode arms. Titanium electrode arms and Au contacts were then deposited by RF magnetron sputtering. The nominal thickness of Ti electrode and Au contacts were 120 nm and 100 nm, respectively. Gold was patterned and wet etched with KI-I_2 solution. Then, titanium layer was patterned by plasma etching. The two-metal-electrode was employed since metals such as Au (κ=3.1 W/cmK), Pt (κ=0.716 W/cmK), or Ag (κ=4.29 W/cmK) make the best electrical contact to YBaCuO. Ti makes a higher resistance contact to YBaCuO but has a relatively low thermal conductivity (κ=0.219 W/cmK) and therefore provides a better thermal isolation than if a single, high thermal conductivity Au electrode was used.

Next, the semiconducting YBaCuO thermometer layer was deposited and patterned into pixels using conventional photolithography and wet etching. The nominal thickness of YBaCuO was 350 nm. The trench cuts were then patterned and wet-etched through the $LaAl_2O_3$ and Si_3N_4 layers to expose the polyimide to oxygen ashing in the final step. Next, holes with dimensions of 3×3 μm^2 and 4×4 μm^2 were patterned on top of YBaCuO. Both YBaCuO and $LaAl_2O_3$ were wet etched. Using the same mask, the supporting membrane Si_3N_4, the Ti-absorber and the passivation Si_3N_4 were dry etched to expose the polyimide to oxygen ashing through the holes. Another passivation layer of Si_3N_4 with thickness of 147 nm was deposited to protect YBaCuO during oxygen plasma ashing of the polyimide. The electrical and optical properties of YBaCuO are affected by the oxygen stoichiometry. Oxygen serves as an acceptor, donating hole carriers to conduction, thus lowering the resistivity and TCR. The trench cuts and holes were realigned, patterned and wet-etched. Subsequently, the bonding contacts were patterned and dry etched.

Finally, the polyimide layer was removed by oxygen plasma ashing for 15-18 hours to suspend the YBaCuO pixel and form the thermal isolation structure. In earlier devices, it was found that the microbolometers that underwent a continuous polyimide undercut etch failed due to cracking when current biased. By interrupting the undercut etch procedure every 30 minutes, the stress-cracking problem was eliminated.

Prior to bonding and packaging of the devices, two-probe resistance measurements were performed on each device across the wafer. Devices with an area of 0.4×0.4 mm^2 and 1.5×1.5 mm^2 utilized 10x380 μm^2 and 0.01x1.48 mm^2 Au contacts to the YBaCuO thermometer, respectively. The two-probe, room temperature, resistance for most of the devices ranged from 1.5 MΩ at the center of the wafer to higher values at the edges, with an average of about 2.0 MΩ. The *I-V* characteristics showed ohmic behavior up to 7 μA with no evidence of significant Joule heating.

Current-voltage (*I-V*), resistance versus temperature (*R-T*), and TCR measurements were performed by mounting the devices in a closed-cycle refrigerator evacuated to 50 mTorr. A HP 4142B Modular DC Source/Monitor Unit was used to measure the *I-V* characteristics. Figure 16 shows a typical *R-T*, the corresponding TCR versus temperature, and *I-V* characteristics. The two-probe TCR was measured over the temperature range of 240 to 320 K. TCR of the 400 × 400 μm^2 and 1.5×1.5 mm^2 size devices were approximately 2.88 $\%K^{-1}$ and 2.74 $\%/K^{-1}$ at 296 K. This value is somewhat lower in magnitude than previously measured values on similar samples for this material which had TCR of 3.5 $\%K^{-1}$. The small difference in TCR is attributed to the exposure of YBaCuO thermometer to the oxygen plasma during the ashing of polyimide to form the suspended structure.

The thermal conductance of the microbolometers was measured by the method of resistive or joule heating at different substrate temperatures. The following relation was employed to calculate *G*:

$$R(T) = R_o + \frac{1}{G}\frac{dR}{dT} I_b^2 R(T) \qquad (3)$$

Here, R_o and *R(T)* are the resistance values at low and high bias currents, respectively. The *dR/dT* is calculated from R-T measurements. It was also measured again with Hewlett-Packard 4142B Modular DC source/Monitor unit at a constant current of 2 μA (high bias). The resistance at different currents ranging from -4 μA to 4 μA was plotted versus dissipated power at constant substrate temperature. The thermal conductance, *G*, was calculated from the slope of this characteristic. The room temperature values of *G* for the small area devices and large area devices were 1.68 $\times 10^{-5}$ W/K and 5.7 $\times 10^{-5}$ W/K, respectively.

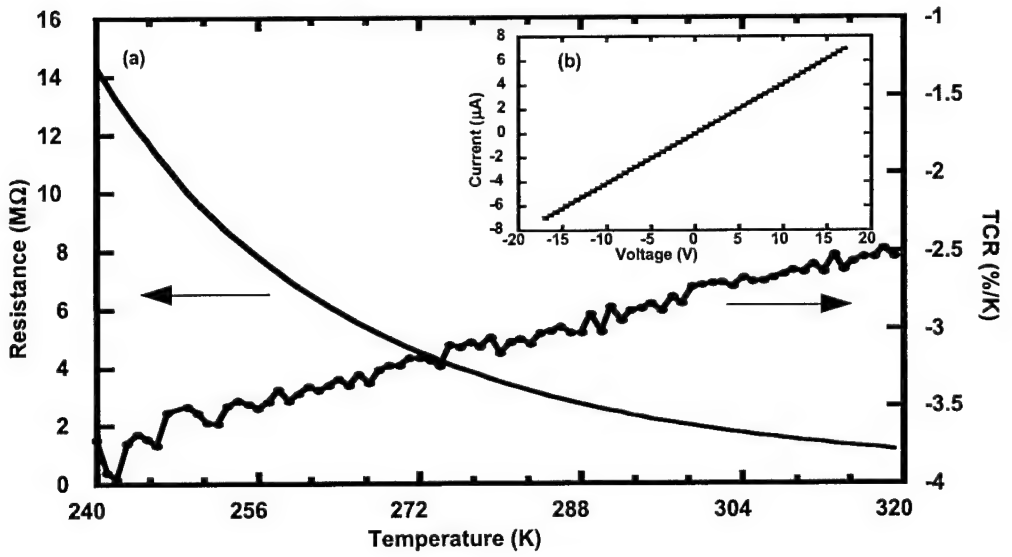

Figure 16. Resistance and temperature coefficient of resistance as a function of temperature over the temperature range of 240 to 320 K for a 400×400 μm^2 microbolometer. The inset displays the linear current-voltage characteristic of the device.

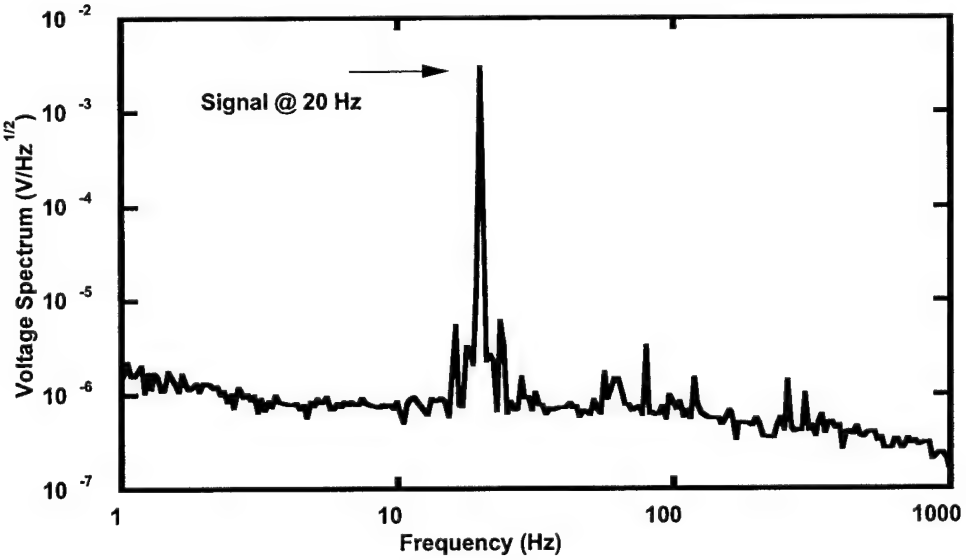

Figure 17. Typical signal spectra from a 1.5x1.5 mm^2 microbolometer. The signal was measured with a current bias of 4.65 μA.

The optical response of the devices was measured by using Oriel 60071 light source housing a 6575 IR ceramic element and 60077 ZnSe condenser/collimator. The radiating element can be modeled as a 1450 K blackbody source. The net usable range of this broadband system was ~0.6-15 μm. The optical power of the broadband source was approximately 6.3 mW/cm^2 for measurements on small area devices and 3.4 mW/cm^2 on large area devices. The room temperature measurements were performed inside an electromagnetically shielded room. The devices were mounted inside a cryostat, allowing the mechanically chopped light to illuminate the sample surface through a ZnSe window. The output voltage was fed into a Hewlett-Packard 3562A dynamic

signal analyzer through a PAR113 preamplifier. The devices were dc biased with currents varying from 0.156 to 10 μA, supplied by a low noise battery-powered current source. The signal analyzer simultaneously measured the signal amplitude and noise per unit bandwidth for each chopper frequency. The response was calibrated with an Oriel 70124 pyroelectric detector. A typical voltage spectrum in vacuum at bias current I_b=4.65 μA is shown in Figure 17. The figure displays a strong voltage response at the chopper frequency of 20 Hz. The power normalized 1/f noise corner frequency was around 0.2 – 0.5 Hz/μW in 400x400μm^2 devices and 1.1 – 1.8 Hz/μW in 1.5x1.5 mm^2 devices. This is considerably lower than the noise exhibited by VO_x and a:Si microbolometers. [34,35]

The responsivity, detectivity and noise equivalent power were calculated from the measured voltage response and noise in vacuum at room temperature and are plotted in Figure 18 as a function of chopper frequency for two bias currents. The NEP reported here is calculated per root Hertz bandwidth for convenience. The measured responsivity and detectivity of the 400 × 400 μm^2 size microbolometers were as high as 1.56×10^3 V/W and 1.27×10^8 cm Hz$^{1/2}$/W at I_b = 4.65 μA, respectively. The noise equivalent power was measured as low as 3.16×10^{-10} W/Hz$^{1/2}$ at the same bias current. For the 1.5 × 1.5 mm^2 size microbolometer, the highest responsivity and detectivity were 180 V/W and 3.07×10^7 cm Hz$^{1/2}$/W at I_b = 5.17 μA, with NEP of ~4.87×10^{-9} W/Hz$^{1/2}$. (Figure 18)

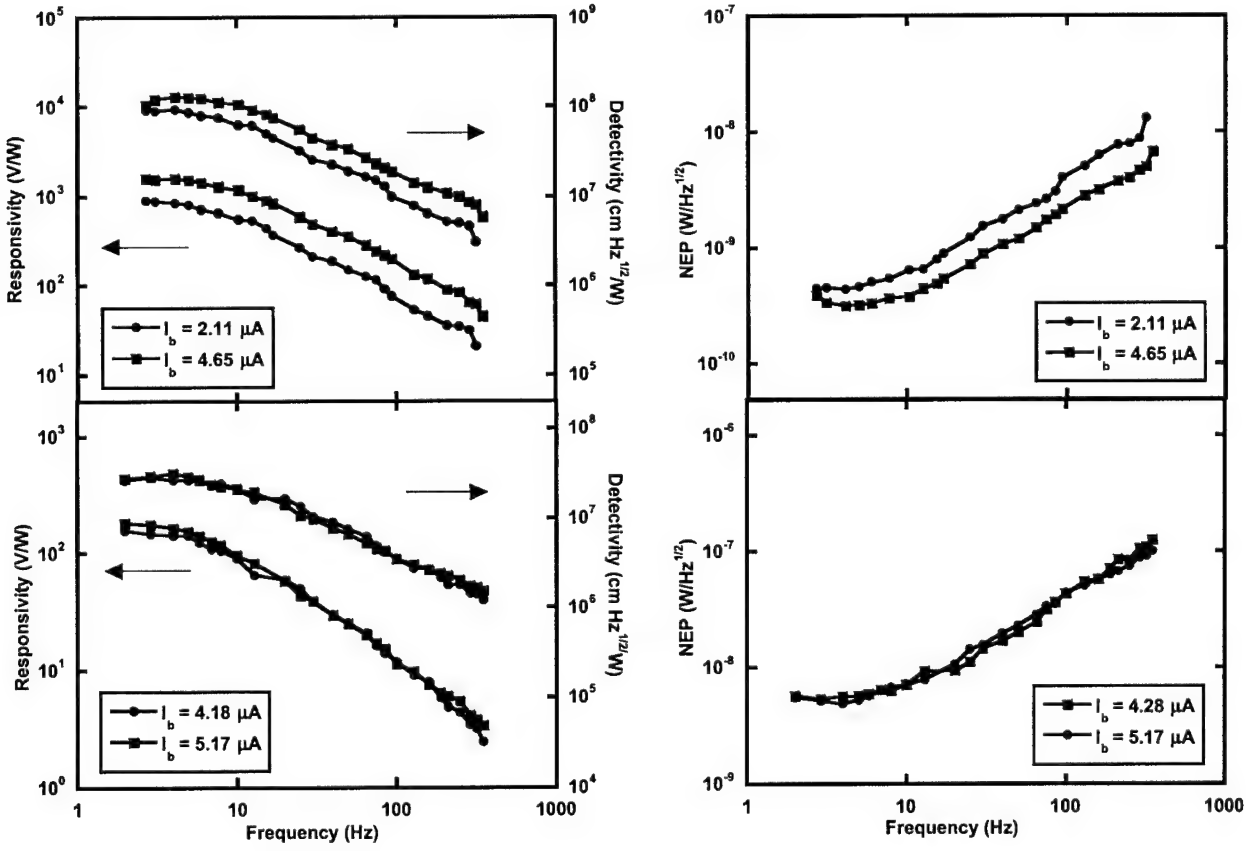

Figure 18. Responsivity, detectivity and noise equivalent power as a function of chopper frequency at different current bias values measured in vacuum with 0.6 to 15 μm broadband IR radiation. The characteristics of 400μm ×400 μm size microbolometer are shown in top figures, while the figures at the bottom are for the 1.5 mm × 1.5 mm size microbolometer.

The spectral response was measured in vacuum as a function of IR wavelength over the range 0.6-15 μm with an Oriel monochromator, and blackbody source. The spectrum displays mixed absorption resonance

that is believed to result from the air gap and the relatively thick layers of YBaCuO and Si_3N_4. The spectral response was relatively flat over the measured wavelength band. The spectral response shows an order of magnitude variation over the wavelength range, largely because of the low absorption in the 4 to 8 μm band. The model predicted approximately a factor of four variation in the absorption over this wavelength range. The differences between the predicted absorption and the measured one can be attributed to inaccuracies in the assumed optical properties of the thin film materials employed and differences between the fabricated and calculated thickness of the thin films. Another factor that undoubtedly affected the absorption characteristics is the partial oxidation of the Ti absorber by the oxygen plasma used to undercut the microbolometers. As a result of optimizing the fabricated device structure, the absorption in the microbolometers was improved from immeasurably small to its current value shown in Fig. 19. With further optimization of the device structure, increased absorption in this wavelength range is possible, providing a flatter spectral response. Improvement in the microbolometer responsivity, detectivity and noise equivalent power requires a decreased thermal mass to shorten the thermal time constant and perhaps also allow for a reduction in the thermal conductance. By fitting the responsivity data into Eq. (1), the values for G/η were calculated to be 2.59×10^{-5} W/K and 1.12×10^{-4} W/K for the small area and large area devices. The thermal time constant, τ_{th} ranged between 13-15 ms and between 25-28 ms for the small area and large area devices, giving a thermal mass C of 2.52×10^{-7} J/K and 1.47×10^{-6} J/K, respectively. The absorptivity was calculated from the fitted G/η value and the measured G to be 58.8% for the small devices and 50.8% for the large devices. This represents a relatively strong IR absorption for the broadband YBaCuO thermometer, comparable to the predictions of the transmission line model used to design the structures. A summary of the measured and extracted characteristics is presented in Table IV.

Table IV. Summary of the results for 400μm ×400 μm 1x4 arrays and 1.5 mm × 1.5 mm single pixel detectors.

Device area	400×400 μm^2	1.5×1.5 mm^2
2-Wire resistance at 295 K (MΩ)	2.42	2.0
TCR (%/K)	2.88	2.74
Thermal conductance G (W/K)	1.68×10^{-5}	5.7×10^{-5}
Thermal capacitance C (J/K)	2.52×10^{-7}	1.47×10^{-6}
Thermal time constant τ_{th}(ms)	15	25.8
Maximum responsivity R_v (V/W)	1.56×10^{3} @ 4.65 μA	180 @ 5.17 μA
Maximum detectivity D^* (cm $Hz^{1/2}$/W)	1.27×10^{8} @ 4.65 μA	3.07×10^{7} @ 5.17μA
NEP (W/$Hz^{1/2}$)	3.16×10^{-10} @ 4.65 μA	4.87×10^{-9} @ 5.17 μA
Absorption (%)	58.8	50.8

Novel room-temperature broadband microbolometers were designed and fabricated by RF magnetron sputtering using a polyimide sacrificial layer and conventional micromachining techniques, fully compatible with post-CMOS processing. This work demonstrates that high performance, large area YBaCuO microbolometers can be produced for radiometric measurements. The microbolometers were fabricated on a 350 nm Si_3N_4 supporting membrane suspended 6.41 μm above the substrate. A double-mirror structure was designed to achieve a relatively uniform absorption up to 100μm wavelength. The microbolometers exhibited a relatively strong absorptivity, ~ 59 % in the 0.6-15 μm wavelength band. The 400×400 μm^2 1x4 microbolometer arrays displayed responsivity and detectivity of 1.56×10^{3} V/W and 1.27×10^{8} cm $Hz^{1/2}$/W, respectively, at a bias current I_b = 4.65 μA. The large area single pixels (1.5 ×1.5 mm^2), on the other hand, had responsivity of 180 V/W and detectivity of 3.07×10^{7} cm $Hz^{1/2}$/W at I_b = 5.17 μA. The measured noise equivalent power was 3.16×10^{-10} W/$Hz^{1/2}$ for small size arrays whereas, the large area single pixels showed NEPs of 4.87×10^{-9} W/$Hz^{1/2}$. The power normalized 1/f noise corner frequency was less than or equal to 2 Hz/μW for large area detectors, while much smaller values, (<1 Hz/μW) were observed on small area detectors. This is a significant improvement in performance for the broadband microbolometer technology. The exposure of the YBaCuO thermometer to the oxygen plasma during the undercut etch is believed to have resulted in a slight reduction of the TCR of the thermometer to around –2.7 –2.8 %/K. The thermal time constant was a factor of 2 to3 larger than the targeted time constant due to the large size and therefore large thermal mass of the microbolometers. The thermal time constant can be decreased by reducing the thickness of the supporting Si_3N_4 layer. However, since these are rather large micromachined structures, this might potentially increase the risk of

warping and wrinkling of the suspended bridge. Finally, further improvement in the spectral response can be achieved by using multimirrors and multiabsorbers.

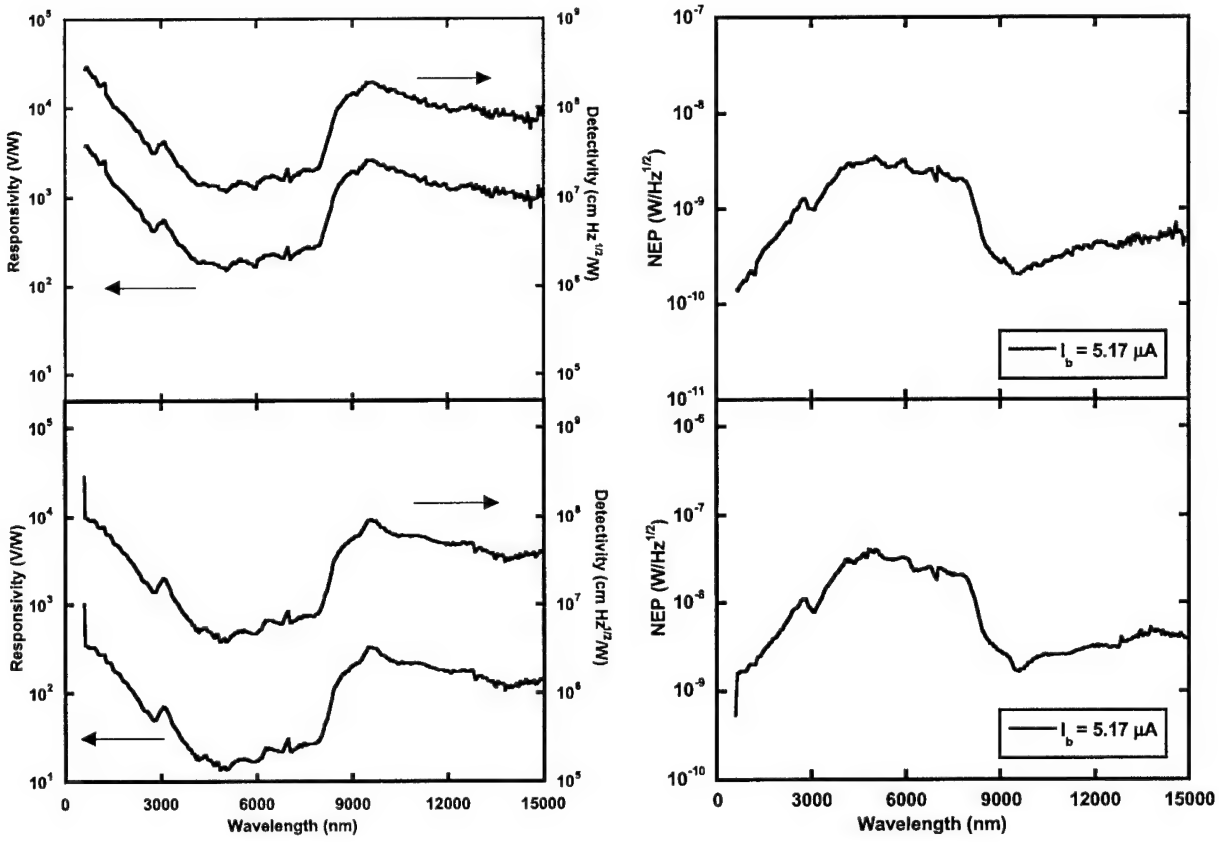

Figure 19. Measured responsivity and detectivity as a function of wavelength of 400μm ×400 μm size (top) and a single pixel with 1.5 mm × 1.5 mm size (bottom).

Micromachined, Two-color Infrared Detectors with Thermal Chopping

A theoretical investigation of two-color infrared detection using a moveable mirror to change the depth of the optical cavity and thermal chopping to provide a fast thermal reset. The resonance between the incoming and reflected waves in the micromachined cavity under the pixel is wavelength-dependent, so the detector can be tuned to a particular spectral band by varying the cavity depth. This property can be utilized to design a multi-color microsensor structure, tunable to two or more selected atmospheric transparency windows by an electrostatically actuated mirror under the pixel.

In the proposed design, the mirror switches between two positions at a rate double the camera frame rate, thus changing a resonant cavity depth and providing response to two wavelength windows in turn. To separate responses in the windows, the read-out also has to be performed at a twice the frame rate. The image can then be integrated at the read-out level to achieve a multi-color picture at the standard 30 Hz frame rate.

The design described above requires doubling of the chopping frequency thereby decreasing detectivity. In order to achieve the required chopping frequency and maintain 30 Hz frame rate, thermal chopping instead of optical or electronic chopping may be used. For this purpose, an actuated thermal microchopper is formed by a thermally conducting cantilever beam that contacts the detector pixel immediately

after each read-out process, i.e. 60 times per second, providing a faster thermal reset to its initial unheated (by IR radiation) state. The second half period, i.e. 1/60 s, usually used to cool the detector, can now be utilized for a measurement in another spectral range. Therefore, the thermal properties of a two-color FPA can be maintained to be the same as that of a one-color array.

At present, IR FPAs utilizing microbolometers demonstrate the best NETD [36]. The only problem with these arrays is related to the bias requirement that causes (i) $1/f$ low-frequency current noise and (ii) temperature drift of the signal offset and responsivity due to the dissipation of electrical power in array. The noise problem is related to both the electrical contact and the bolometer resistance fluctuations. It is solvable only through the implementation of improved materials for the thermometer and contact. Self-heating of the arrays and the related drift of the output signal offset is a more serious problem. Staring microbolometer arrays require precise temperature stabilization [6] to maintain a calibrated response. This can be done by maintaining a stable temperature with the combination of a heater and thermoelectric cooler or Peltier effect. Another possible approach is to perform compensation of self-heating at the read-out electronics level [37]. Chopping of radiation at doubled frame rate allows offset correction, but this leads to a decrease in detectivity.

The power reaching the detector, P_D is significantly less and can be written down as:

$$P_D = \frac{A}{4F^2}\int_{\lambda_1}^{\lambda_2} \frac{2\tau_{atm}(\lambda)\tau_{obj}(\lambda)\pi hc^2\varepsilon(\lambda)\eta(\lambda)}{\lambda^5(e^{hc/\lambda kT_{sc}}-1)}d\lambda \tag{4}$$

where A is the detector (pixel) receiving area, F is the focal ratio of the objective, $(\lambda_1 - \lambda_2)$ is the atmospheric window or optically limited band, $\tau_{atm}(\lambda)$ and $\tau_{obj}(\lambda)$ is the transmissivity of atmosphere and objective, $\eta(\lambda)$ is the detector absorptivity.

However, even Eq. (5) does not reflect useful optical power, i.e. the power that can be interpreted in terms of the temperature resolution between objects in the scene. Indeed, the primary goal is to detect the relative temperature of objects in the scene rather than the absolute temperature. Assuming there is an object with another temperature, $T_{obj}=T_{sc}+\Delta T_{sc}$ in the field of camera view. The IR power received in the optical band λ_1 to λ_2 by an array pixel looking at this object $P_{D2}=P_D+\Delta P_D$, and its increase is

$$\Delta P_D = \frac{A}{4F^2}\int_{\lambda_1}^{\lambda_2} 2\frac{\tau_{atm}(\lambda)\tau_{obj}(\lambda)\pi hc^2\varepsilon(\lambda)\eta(\lambda)}{\lambda^5}\frac{\partial}{\partial T_{sc}}\left(\frac{1}{(e^{hc/\lambda kT_{sc}}-1)}\right)\Delta T_{sc}d\lambda \tag{5}$$

For further discussion, we denote the spectral radiant exitance

$$M(\lambda,T_{sc}) = \frac{2\pi hc^2}{\lambda^5(e^{hc/\lambda kT_{sc}}-1)} \tag{6}$$

assuming that

$$\int_{\lambda_1}^{\lambda_2}\tau_{atm}(\lambda)\tau_{obj}(\lambda)\varepsilon(\lambda)\eta(\lambda)\frac{\partial M(\lambda,T_{sc})}{\partial T_{sc}}d\lambda = \left(\tau_{atm}\tau_{obj}\varepsilon\eta\frac{\Delta M}{\Delta T_{sc}}\right)_{\lambda_1-\lambda_2} \tag{7}$$

where τ_{atm}, τ_{obj}, ε and η are the transmission, emission and absorption within the $(\lambda_1 - \lambda_2)$ region, $(\Delta M/\Delta T_{sc})_{\lambda_1-\lambda_2}$ is the temperature contrast, i.e. the change of IR power radiated per unit area of a blackbody within the $(\lambda_1 - \lambda_2)$ region if its temperature changes by ΔT_{sc}. Simplifying Eq. (5), one can obtain the change of detected power in the wavelength range λ_1 to λ_2, P_{D2} per ΔT_{sc} as:

$$\frac{\Delta P_D}{\Delta T_{sc}} = \frac{\tau_{atm}\tau_{obj}\varepsilon\eta A}{4F^2}\left(\frac{\Delta M}{\Delta T_{sc}}\right)_{\lambda_1-\lambda_2} \tag{8}$$

The responsivity must be maximized for the atmospheric IR transparency window of 8 to 14 μm by the appropriate design of the optically resonant cavity. For a suspended detector pixel, (Fig. 20), the optically resonant cavity depth d plays an important role in the absorption of radiation if the detector is semi-transparent and d is comparable with λ. In this case, the absorption of the detector dramatically increases due to the resonance between the incoming and reflected waves if $d \approx \lambda/4+\lambda n/2$, where n is an integer. Conventional tuning of the resonant cavity in the modern IR arrays occurs at $d \approx 2$ μm providing effective absorption over the entire 8

– 14 μm window. The tuning can be significantly changed if the cavity depth increases. At $d \approx 4$ μm, the detector effectively absorbs IR power only within the long-wavelength half window, while at $d \approx 6$ μm the detector absorbs in the short-wavelength half window. This property of the resonant cavity is used in this work to create a two-color detector model. In order to tune the detector from one spectral band to the other spectral band inside the 8 – 14 μm region, the mirror under the pixel should be movable. It can be actuated electrostatically, using standard MEM device techniques since the mirror requires a motion of only 1.5-μm.

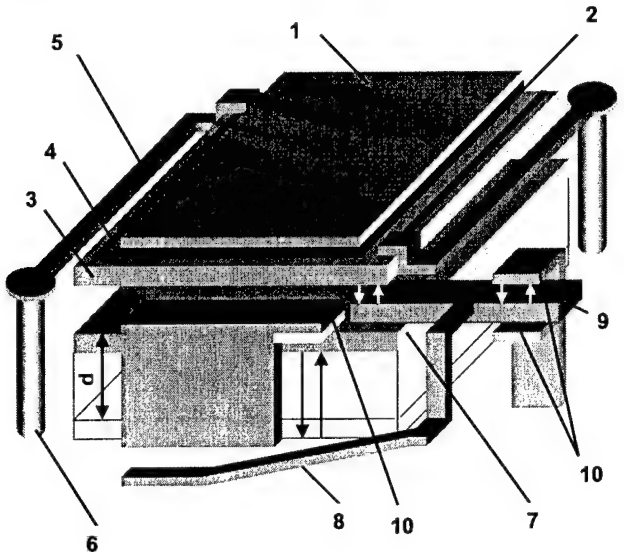

Figure 20. The schematic for proposed design of two-color floating detector with thermal MEM-chopper: (1) Ti absorber, (2) SiO_2 insulator, (3) bolometric Si film, (4) Au electrode, (5) Ti leg, (6) W pillar, (7) free mirror, (8) Al cantilever beam (bending part of the chopper), (9) thermally conducting part of the Al chopper covered with Si_3N_4 insulating film, (10) electrostatic actuating plates.

The spectral properties of resonant cavity were calculated using a transmission line theory [38] for the case of normal incidence of the radiation. In order to optimize the detection properties, the thermal, electrical, material, mechanical and thermal-conversion properties were simultaneously optimized along with the optical properties. The absorptivity is shown in Fig. 21.

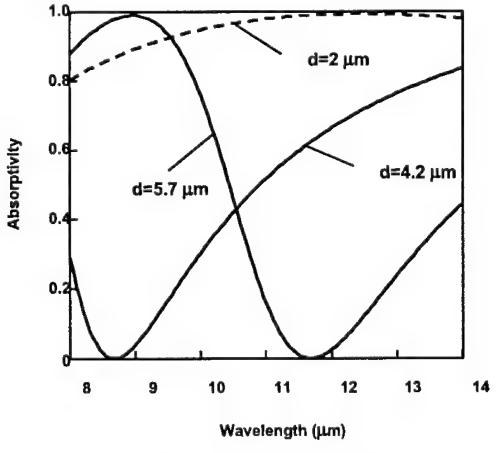

Figure 21. Optical tuning of the resonant cavity in LWIR region. Dotted line shows conventional tuning for the whole 8 – 14 μm window. Solid lines show proposed tuning providing a selection of the 8 – 10.5 μm or 10.5 – 14 μm regions.

Calculation of the temperature contrast $(\Delta M/\Delta T_{sc})_{\lambda_1-\lambda_2}$, Fig. 22, was performed based on Eqs. (46) and (5). From Fig. 22, the temperature dependence of $(\Delta M/\Delta T_{sc})_{\lambda_1-\lambda_2}$ differs between the 8 – 10.5 μm and 10.5 – 14 μm subbands. Defining $\Delta P_{8\text{-}10.5\ \mu m}$ and $\Delta P_{10.5\text{-}14\ \mu m}$ as ΔP_D calculated for the cavity heights of d = 5.7 μm and d = 4.2 μm respectively, the ratio $\Delta P_{8\text{-}10.5\ \mu m}/\Delta P_{10.5\text{-}14\ \mu m}$ will also change with the object temperature. Total power radiated by the unit surface of the blackbody object in the same spectral regions was calculated using Eq. (4) assuming $\varepsilon(\lambda)$=1 for a blackbody. An important point to consider for the radiance $M(T_{sc})_{\lambda_1-\lambda_2}$, the contrast $(\Delta M/\Delta T_{sc})_{\lambda_1-\lambda_2}$, and the ratio $\Delta M_{8\text{-}10.5\ \mu m}/\Delta M_{10.5\text{-}14\ \mu m}$ is the redistribution of the IR power between the sub-regions with the blackbody temperature. The change of the ratio $\Delta M_{8\text{-}10.5\ \mu m}/\Delta M_{10.5\text{-}14\ \mu m}$ allows the measurement of the object's temperature by comparing the responses in the two sub-regions.

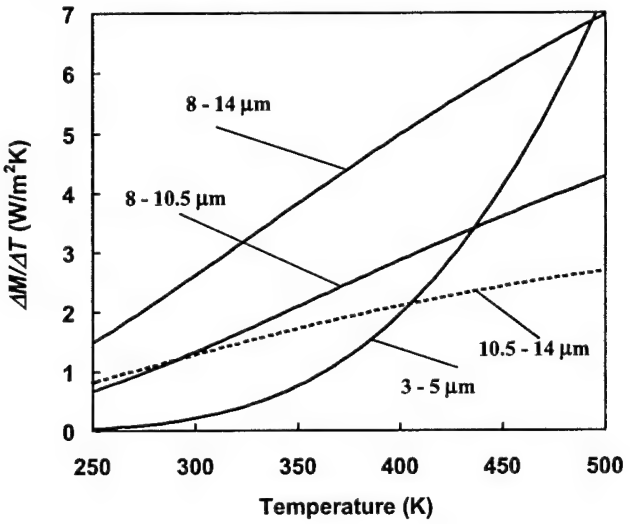

Figure 22. Temperature dependence of the temperature contrast in the different spectral regions: (1) 8 – 14 μm, (2) 8 – 10.5 μm, (3) 10.5 – 14 μm, (4) 3 – 5 μm .

The thermal time constant (response time) of detector is $\tau = R_{th}C_{th}$ where C_{th} is the heat capacity of the detector. A R_{th}=10^8 – 10^9 K/W is necessary for the background-limited NETD at room temperature, requiring the heat capacity and thickness of the detector pixel to be minimized to achieve τ<5 ms for a 30 Hz frame rate. Optimization of the detector structure for mechanical stability, low heat capacity of the pixel and legs, high thermal resistance and electrical conductance of the legs, good IR absorption and low detector noise combined with the goal of high responsivity have led to the final decision concerning materials and the size of detector elements. The detector was optimized for the two-color geometry discussed in this paper, Fig. 20. Fig. 23a) and 23b), show the calculated voltage versus time signal diagrams for the detector when used with a conventional mechanical chopper. The rotating chopper wheel opens the detector for exposure to IR radiation, Fig. 23a), for half the 1/30 s frame cycle. The corresponding cooling and heating exponential signals of detector are shown in Fig. 24b). An attempt to increase the chopping frequency by a factor of two to measure the radiant energy in two spectral regions during the same frame period decreases the output signal, thereby decreasing the detectivity D^* and increasing NETD.

To maintain the same D^* in a two-color camera while simultaneously maintaining the same thermal time constant τ and frame rate as in a one-color camera, an extra-fast thermal return into the initial, unheated state is required. Therefore, instead of a slow detector cooling cycle during half the period of the mechanical chopping, thermal chopping is being proposed to provide a fast cooling cycle. For this purpose, an electrostatically actuated cantilever beam with low thermal resistance is incorporated into the detector, Fig. 20, providing periodic thermal contact to the pixel, thereby providing a good heat sink and dramatically decreasing the high thermal resistance of the detector. We have named such a cantilever beam a "thermal chopper". The

contact of the cantilever causes the cooling of the detector as occurs when it is shielded from radiation by a conventional, mechanical chopper. This thermal chopper could also be implemented in staring microbolometer arrays to provide a thermal reset. In staring arrays, an interlaced reset scheme could be implemented to allow the camera to continuously operate.

So, even 1% of the frame period can be enough for the cooling instead of half period in the modern FPA. So, the proposed design allows measurements in the two spectral regions with the same frame rate and D^* as in the one-color case. A corresponding time diagram for the thermally chopped case is shown in Fig. 23c). The FPA will show a dramatic reduction in the tracks of hot objects even if about 2 – 3% of the frame period is used for a cooling cycle instead of 1%. In order to eliminate possible microphonic effect, the special durable design for the legs will be required for detectors.

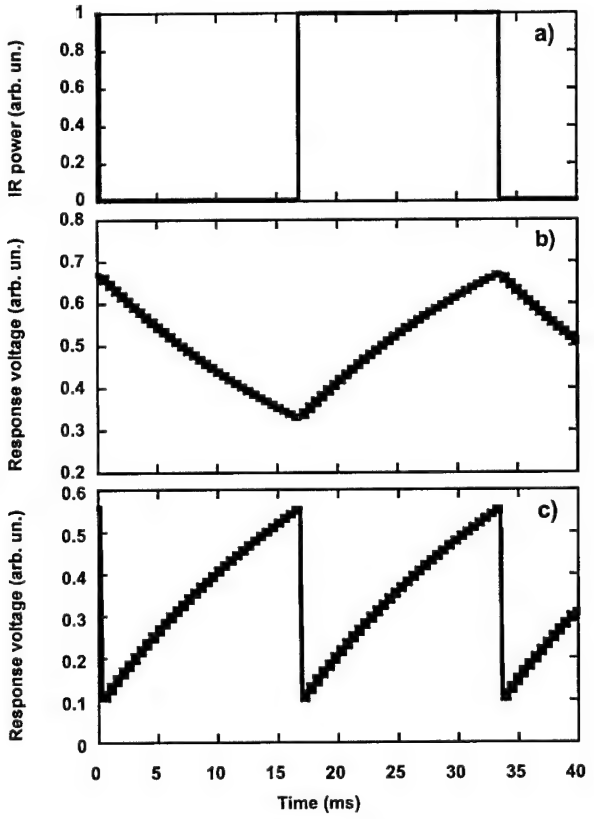

Figure 23. Calculated time diagrams for the detector operation: (a) optical power modulated by conventional chopper, (b) and (c) are response diagrams in optical and thermal chopping regime, respectively.

Calculation has shown that the multi-color detection with uncooled IR FPA can be performed using a tunable resonant cavity under the detector. "Coloring" of the IR with the proposed FPA design is available with two incorporated microactuators, i.e. a moving micromirror and a thermal microchopper. The actuated micromirror tunes the detector to different spectral regions each 1/60 s, in the case of standard American video frame rate. The thermal chopper ensures a faster cooling of the detector than exists in the modern FPA (about 240 times faster in this particular design). Therefore, the second half frame period formerly used for cooling detector now is used for the measuring in the second spectral region. Background-limited NETD at the few-mK level is expected. The particular design shows calculated NETD=1.1 and 1.2 mK (for an electrical bandwidth Δf =1 Hz) in two spectral bands, i.e. 8 – 10.5 μm and 10.5 – 14 μm. respectively, when 30 Hz frame rate is being used. At 300 K, the color separation, i.e. the distance between the maxima for the spectral density of absorbed IR power is 4.22 μm in this particular case. The 19%-offset at the read-out level allows total color separation, with no cross-reference color mixing.

The technical challenge in the proposal will be to produce a mechanically sound implementation of the concepts. The striking of the pixel with a thermal chopper will provide mechanical stress to the pixel. It is

believed that the magnitude of the stress will not be severe since the thin film arm will be itself delicate and easily pliable. The moveable mirror would similarly undergo distortion and not remain perfectly flat as assumed in this model, as it is shifted from one position to another. The distortion should be reproducible from cycle to cycle causing the precise spectral dependence of the absorption to differ from this model but the contrast allowing two-color imagery would remain.

New self-supporting detectors have been designed which will reduce the thermal mass and lower the thermal conductivity by two orders of magnitude to increase the responsivity and the detectivity by one to two orders of magnitude. Several arm shapes were designed with deflection less than 10 % for this purpose. In addition, the current mask set was redesigned, the dimensions and shapes of the arms were changed. One of the new designed pillar structure detectors is shown in Figure 24.

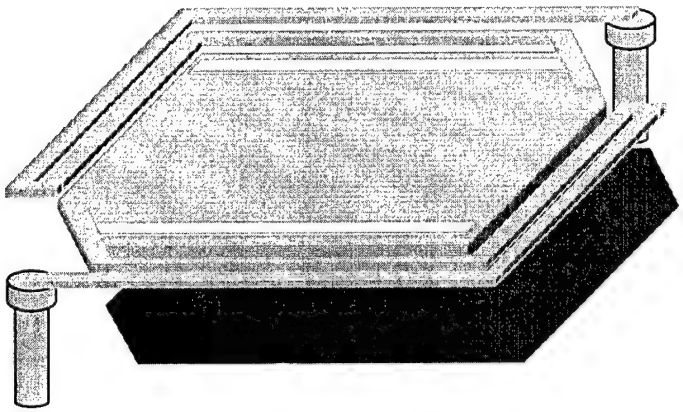

Figure 24. Improved Pixel design

The maximum responsivity and detectivity calculated for these structures are 5.2×10^5 V/W and 9.5×10^9 cm $Hz^{1/2}/W$, respectively. The NETD improved to a value less than 2 mK. The NETD is plotted vs. frequency in Figure 25.

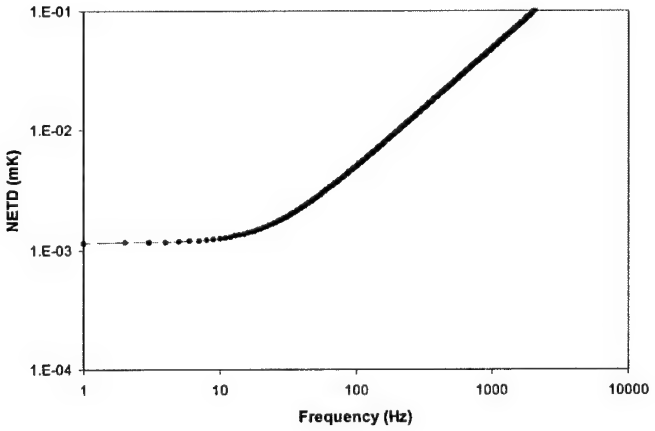

Figure 25. NETD versus frequency, the band width is 1 Hz, Transmittance 0.9 and F is 1

These detectors have been fabricated, however, at the time of writing this report the characterization and analysis of the data has not been completed. SEM micrographs of some of the detectors with long meandering electrode arms are shown in Fig. 26.

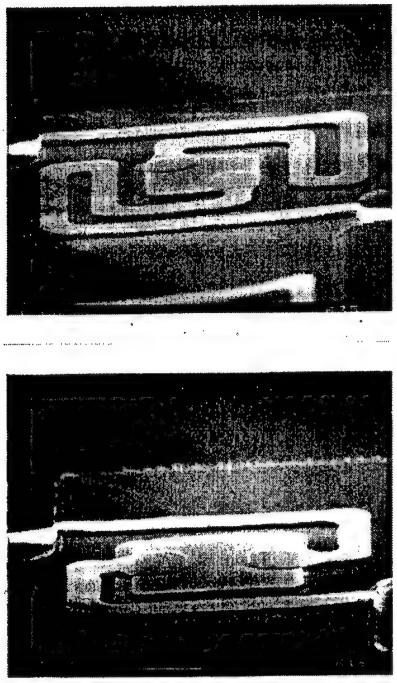

Fig. 26 SEM of 40x40μm^2 self-supporting YBaCuO microbolometers with Ti electrode arms and Au contacts.

II-2C. MAJOR FINDINGS FOR TASK 3:

The new generation of uncooled focal plane arrays caused revolutionary changes in both commercial and defense applications of uncooled infrared (IR) imaging. The noise equivalent temperature difference (NETD) is a generally accepted measure of sensitivity for these IR imagers [39]. Recently, NETD as low as 14 mK has been demonstrated by Raytheon Systems Company [40], and further improvements are expected down to the theoretical limit of background limited NETD [41].

The current production of military and commercial infrared imaging systems at Raytheon is based on hybrid ferroelectric technology [42]. These systems are built around 240×320 imaging arrays with pixels on 48.5-μm centers and show NETD as low as 38 mK [43]. However, current technology has some limitations on further improvement. Recently, monolithic ferroelectric technology has been successfully demonstrated as a viable alternative to hybrid technology [44]. Such technology offers a potential for NETD as low as about 1 mK, i.e., significantly better than about 20 mK, the potential to achieve with hybrid technology [45].

One of the promising candidates as a pyroelectric detector material for such a technology is modified lead titanate. This investigation is devoted to impedance and dielectric loss noise measurements on arrays of 240×320 self-supporting micromachined capacitor structures with modified lead titanate as the IR sensitive pyroelectric film. These arrays are gangs of 10 and 100 pixels connected together in parallel.

The investigation consisted of two parts: the first is $\tan\delta$ measurements; and the second one is related to both calculation of $\tan\delta$ noise using measured $\tan\delta$ and direct noise measurements on the pyroelectric detectors. The parameters of four arrays were measured; #1 and #2 consist of 100 pixels, #3 and #4 consist of 10 pixels, 40x40 μm^2 in area.

A summary of parameters measured on the Raytheon IR detector arrays is shown in Table V.

The first part of the experiment was carried out at room temperature (297 – 300 K) and at residual air pressure of 21 – 70 mTorr. The impedance measurement results are shown in Fig. 12. Arrays show similar behavior for capacitance, i.e., the relative real permittivity is the same for all arrays. However, the loss resistivity decreases with the number of pixels proportionately in only three arrays. The array #1, the only exception, exhibits much less loss resistance than expected, e.g., more than two orders of magnitude less than others at the frequencies below 10 Hz.

Table V. Parameters of arrays at the frequency of 30 Hz and the temperature of 300 K.

Parameter	Array #			
	1	2	3	4
ρ, Ω m	3.0×10^7	3.7×10^8	2.4×10^8	3.2×10^8
ε'	43	37	39	35
$\tan\delta$	0.46	0.045	0.054	0.064

Temperature dependence of the impedance was measured for 220 – 340 K at 20 K intervals. As in the case of room temperature, the real permittivity was not a function of frequency at low temperatures. The real part of relative permittivity and loss tangent at different frequencies are displayed in Fig. 27. Around 300 K, the capacitance per pixel increases with temperature only by 0.003 pF/K. In terms of real permittivity this translates into an increase of only 0.12 %/K. Although the real component of the relative permittivity is almost insensitive to temperature, the loss tangent behavior implies a dielectric relaxation process. The peak displayed by $\tan\delta$ shifts to higher temperatures for higher frequencies. This behavior is similar to that reported for pyroelectric Nb/Y-Ba-Cu-O/Nb structures [33], where the relaxation of polarization was observed in Y-Ba-Cu-O real permittivity.

Using the measured $\tan\delta$ the noise magnitude was calculated for all four arrays (Fig. 28). The scattering of the points is caused by the error in the measurement of relatively large R_d values. The lines are least squares fit to the points. For all arrays, corresponding values of noise voltage are less than Johnson noise of the load resistor and/or noise of the preamplifier at all frequencies.

The temperature dependence of noise was also investigated and it was found that the measured system and array noise components agreed with those calculated ones for all temperatures between 220 and 340 K. As predicted, the array noise was well below the system noise for #2, #3 and #4, whereas, for the "lossy" array #1, the device noise was distinctly observable above 280 K. (Fig. 29). It should be noted that the exhibited noise at 1 Hz is in the order of a $fA/Hz^{1/2}$ per pixel for a 70-pA bias current, a very low noise value.

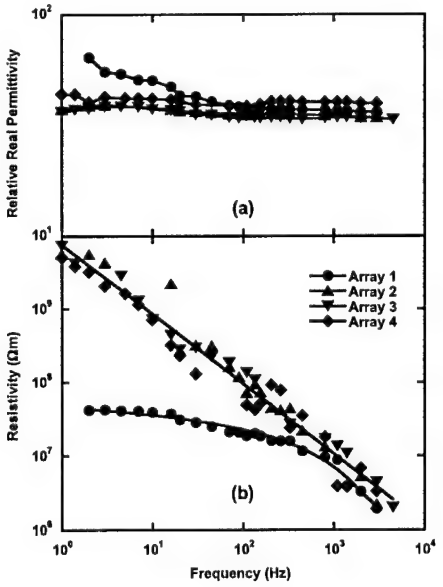

Figure 27. Frequency dependence of (a) relative real permittivity and (b) resistivity of the modified lead titanate arrays at 300 K. Lines in (a) are guides for the eye; lines in (b) are least-squares fit to the data.

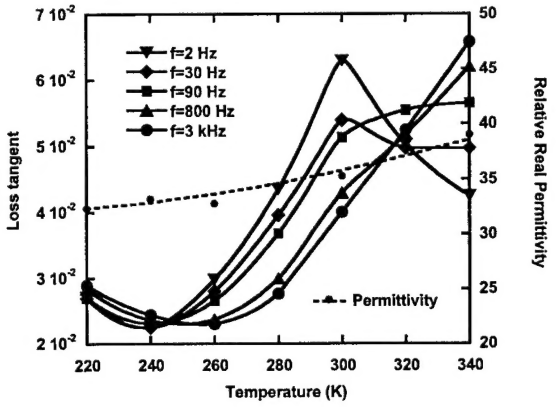

Figure 28. Temperature dependence of relative real permittivity for array #3 at f= 30 Hz and loss tangent at different frequencies. Solid lines are obtained through the interpolation of tanδ between experimental points; dotted line is the least squares fit to the relative real permittivity.

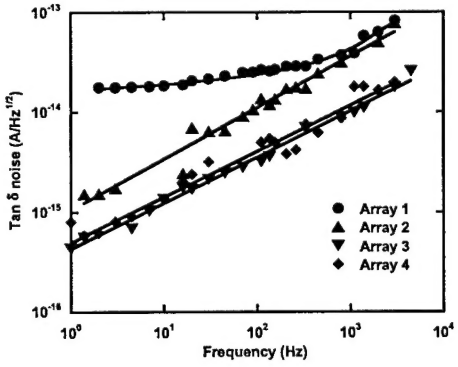

Figure 29. Calculated frequency dependence of tanδ noise current at 300 K. The lines are obtained through the calculation of noise components using the fitted dependence for array resistivity.

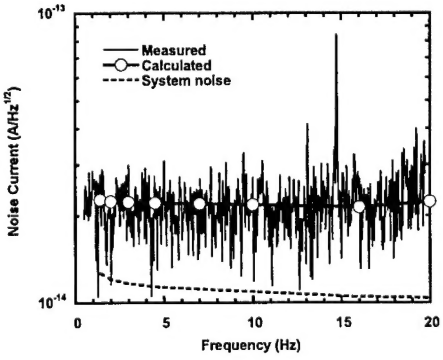

Figure 30 Dependence of the noise current power spectral density at 1 and 10 Hz on bias current for array #3. R_f=10 MΩ, T_d=300 K.

II-2D. MAJOR FINDINGS FOR TASK 4:

Raytheon was successful in demonstrating thin film pyroelectric focal plane arrays using modified lead titanate detectors before its program was terminated and the group disbanded. The end of the Raytheon program made the cost of producing YBCO focal plane arrays prohibitive without the participation of Raytheon in this program. A side note, Mitsubishi recently reported on its independent (without any help from SMU) development of uncooled YBCO microbolometer focal plane arrays with an NETD of 70 mK. SMU has obtained funding from NASA to develop micro-pyroelectric detectors with on chip readout. At present, a scanned IR camera with external readout circuitry is being developed at SMU. The software for the camera is currently being refined in order to obtain imagery. The laboratory camera will allow imagery to be produced from the prototype detectors.

Dr. Celik-Butler and Dr. Butler have also received a grant from NASA to develop broadband FIR pyroelectric detectors with on-chip readout to continue this work. In this case, the CMOS readout circuit will be designed at SMU and fabricated at a foundry. The detectors will then be fabricated on the CMOS substrates at SMU.

REFERENCES

[1] Heavens O. S. Optical Properties of Thin Solid Films. Dover: New York, (1965).

[2] Hass G. and Scott N. W. "On the Structure and Properties of some Metals and Metal Oxide Films." in Selected Papers on Deposition of Optical Coatings, Edited by M.R.Jacobson, SPIE Publ., 1989.

[3] Hahn R. E. and Seraphin B. O. "Spectrally Selective Surfaces for Photothermal Solar Energy Conversion." in Physics of Thin Films, Edited by Georg Hass, Academic Press, 10, 1978.

[4] Buncick M. C. and Denton D. D. "Effects of Aging on Polyimide: A Study of Bulk and Interface Chemistry." Solid State Sensors and Actuators Workshop: 4th Technical Digest, IEEE. 1990, pp. 102-106.

[5] Lide D. R., Editor, Handbook of Chemistry and Physics, 73rd Edition, 1992-93.

[6] Bly V. T. and Cox J. T. "Infrared Absorber for Ferroelectric Detectors." Appl. Optics. 1994, 33(1), pp. 26-30.

[7] Parsons A. D. and Pedder D. J. "Thin Film Infrared Absorber Structures for Advanced Thermal Detectors." J. Vac. Sci. Tech. A. 1998, 6(3), pp. 1686-1689.

[8] Hilsum C. "Infrared Absorption of Thin Metal Films." J. Opt, Soc. of America. 1954, 44(3), pp. 188-191.

[9] Bauer S., Bauer-Gogonea S., Becker W., Fettig R., Ploss B., and Ruppel W. "Thin Metal Films as Absorbers for Infrared Sensors." Sensors and Actuators A. 1993, 37-38, pp. 497-501.

[10] Bogachev V. V., Leonov V. N., and Khrebtov I. A. "Thermal Model for High-Temperature Superconducting Antenna Microbolometers." Tech. Phys. Lett. 1994, 20(5), pp. 426-428.

[11] Gray J., Çelik-Butler Z., Butler D. P., Almasri M. "Semiconducting YBaCuO as Infrared Detecting Bolometers." SPIE, 1998, 3436, pp. 555-565.

[12] Jahanzeb A., Travers C. M., Çelik-Butler Z., and Butler D. P. "A Semiconducting YBaCuO for Room Temperature IR Imaging," IEEE Trans. on Electron Devices. 1997, 44(10), pp. 1795-1801.

[13] Gray J. E., Çelik-Butler Z., and Butler D. P. "MgO Sacrificial Layer for Micromachining Uncooled Y-Ba-Cu-O IR Microbolometers on Si3N4 Bridges." IEEE J. Microelectromechanical Systems. 1999, 8(2), pp. 192-199.

[14] Bock J. J., Parikh M. K., Fischer M. L. and Lange A. E. "Emissivity Measurements of Reflective Surfaces at Near Millimeter Wavelengths." Appl. Optics. 1995, 34(22), pp. 4812-4816.

[15] G. Yu and A. J. Heeger, "Photoinduced Charge Carriers in Insulating Cuprates: Fermi Glass Insulator, Metal-Insulator Transition and Superconductivity", *International Journal of Modern Physics B,* **7**, 3751 (1993).

[16] J. D. Jorgensen, B. W. Veal, A. P. Paulikas, L. J. Nowicki, G. W. Crabtree, H. Claus and W.K. Kwok, "Structural Properties of Oxygen-Deficient $YBa_2Cu_3O_{7-\delta}$", *Physical Review B*, **41**, 1863 (1990).

[17] A. A. Aligia and J. Garces, "Charge Transfer and Oxygen Ordering in $YBa_2Cu_3O_{6+x}$", *Physical Review B,* **49**, 524 (1994).

[18] V. E. Zubkus, O. E. Parfionov, E. E. Tornau, and P .J. Kundrotas, " Asymmetry of Phase Diagram and Influence of Oxygen Ordering on Holes Pairing in $YBa_2Cu_3O_{6+x}$", *Physica C,* **198**, 141 (1992).

[19] N. A. Khan, M. Z. Iqbal and N. Baber, "Electrical and Infrared Characterization of the Semiconducting Phases of $YBa_2Cu_3O_{6+x}$", *Solid State Communications,* **92**, 607 (1994).

[20] Z. Çelik-Butler, P. C. Shan, D. P. Butler, A. Jahanzeb, C. M. Travers, W. Kula, and R. Sobolewski, "Charge Transport in Amorphous and Tetragonal Semiconducting YBaCuO Thin Films," *Solid-State Electronics*, **41**, 895 (1997).

[21] D. P. Butler, Z. Çelik-Butler, A. Jahanzeb, J. E. Gray, C. M. Travers, "Micromachined YBCO Capacitor Structures as Uncooled Pyroelectric Infrared Detectors," *Journal of Applied Physics*, **84**, 1680 (1998).

[22] J. Gray, D. P. Butler, and Z. Çelik-Butler, "Semiconducting YBaCuO Pyroelectric Infrared Detectors on Suspended Si_3N_4 Films," *Electronic Letters*, **34**, 2164 (1998).

[23] D. P. Butler, Z. Çelik-Butler, R. Adam, and R. Sobolewski, "Pyroelectric Effect in Y-Ba-Cu-O Thin Films Under Laser Illumination," *Journal of Applied Physics*, **85**, 1075 (1999).

[24] D. R. Zankowsky, "Flat-Panel Display Benefit from Laser Processing", *Laser Focus World*, **30**, 139 (1994).

[25] A. Marmorstein, A. T. Voutsas, and R. Solanki, "A Systematic Study and Optimization of Parameters Affecting Grain Size and Surface Roughness in Excimer Laser Annealed Polysilicon Thin Films", *Journal of Applied Physics*, **82**, 4303, (1997).

[26] V. A. Volodin, M. D. Efremov, V. A. Gritsenko, and S. A. Kochuebi, "Raman Study of Silicon Nanocrytals Formed in SiN_x Films by Excimer Laser or Thermal Annealing", *Applied Physics Letters*, **73,** 1212, (1998).

[27] D. R. Chen, J. S. Luo, W. T. Lin, C. Y. Chang, and P. S. Shih, "Interfacial Reactions of $Pd/Si_{0.76}Ge_{0.24}$ by Pulsed KrF Laser Annealing", *Applied Physics Letters*, **73**, 1355, (1998).

[28] S. Imanaga, H. Kawai, K. Kajiwara, K. Kaneko, and N. Watanabe, "Excimer-Laser Annealed Ohmic Contacts to *n*-GaAs Substrates Through an Ultrathin Reacted Layer", *Journal of Applied Physics*, **62,** 2381, (1987).

[29] I. Bozovic, "Plasmons in Cuprate Superconductors", *Physical Review B,* **42**, 1969, (1990).

[30] C. Stockinger, W. Markovitsch, W. Lang, W. Kula, and R. Sobolewski, "Mechanisms of Photodoping in Oxygen-Deficient $YBa_2Cu_3O_x$ Films Studied by *in situ* Transport Measurements", *Physical Review B,* **57**, 8702, (1998).

[31] G. K. Guist, T. W. Sigmon, J. B. Boyce, J. Ho, "High-Performance Laser-Processed Polysilicon Thin-Film Transistors", *IEEE Electron Device Letters,* **20**, 77, (1999).

[32] Y. Zhu, J. Zhu, Y. J. Song, and S. Desu, "Laser-Assisted Low Temperature Processing of $Pb(Zr,Ti)O_3$ Thin Film", *Applied Physics Letters*, **73**, 1958, (1998).

[33] J. E. Gray, Z. Çelik-Butler, D. P. Butler and A. Jahanzeb, "Dielectric and Pyroelectric Response in Nb/Semiconducting Y-Ba-Cu-O/ Nb Structures", *Ferroelectrics*, **209**, 517, (1998).

[34] C. Marshall, N. Butler, R. Blackwell, R. Murphy, and T. Breen, "Uncooled infrared sensor with digital focal plane array", *Proc. of SPIE* **2746**, pp. 23 – 31, 1996.

[35] B. I. Craig, R. J. Watson, and M.H. Unewisse, "Anisotropic excess noise within a-Si:H," *Solid-State Electronics* **39**, pp.807-812, 1996.

[36] B. Beyer, R. Cannata, A. Stout, A. Gin, P. Taylor, E. Woodbury, J. Deffner, and F. Ennerson, "Amber's Uncooled Microbolometer LWIR Camera," in *SPIE Proc. on Infrared Detectors and Focal Plane Arrays IV*, E.L. Dereniak and R.E. Sampson, Ed., **2746**, 13–22 (1996).

[37] X. Gu, G. Karunasiri, J. Yu, G. Chen, U. Sridhar, and W. J. Zeng, "On-chip compensation of self-heating effects in microbolometer infrared detector arrays," Sens. Actuators A **69**, 92–96 (1998).

[38] S. Ramo, J. H. Whinnery, and T. Van Duzer, *Fields and Waves in Communication Electronics*. (J. Wiley, New York, 1967).

[39] Kruse P.W. Principles of Uncooled Infrared Focal Plane Arrays. In: Uncooled Infrared Imaging Arrays and Systems, Kruse P., Skatrud D., editors. Semiconductors and Semimetals, 1997; 47: 17-42.

[40] Radford W., Wyles R., Wyles J., Varesi J., Ray M., Murphy D., Kennedy A., Finch A., Moody E., Cheung F., Coda R., Baur S., Microbolometer Uncooled Infrared Camera With 20 mK NETD. Proceedings of SPIE. 1998; 3436: 636-646.

[41] Kruse P.W. A comparison of the limits to the performance of thermal and photon detector imaging arrays. Infrared Phys. Technol. 1995; 36: 869-882.

[42] Hanson C., Beratan H., Owen R., Corbin M., McKenney S., Uncooled thermal imaging at Texas Instruments. In: Infrared Detectors: State of the Art, Makky W.H., editor. Proceedings of SPIE. 1992; 1735: 17-26.

[43] Hanson C.M., Beratan H.R., Belcher J.F., Udayakumar K.R., Soch K.L. Advances in monolithic ferroelectric uncooled IRFPA technology. Proceedings of SPIE. 1998; 3379: 60-68.

[44] Belcher J.F., Hanson C.M., Beratan H.R., Udayakumar K.R., Soch K.L. Uncooled monolithic ferroelectric IRFPA technology. Proceedings of SPIE. 1998; 3436: 611-622.

[45] Hanson C.M., Hybrid Pyroelectric-Ferroelectric Bolometer Arrays, Uncooled Infrared Imaging Arrays and Systems, Kruse P., Skatrud D., editors, Semiconductors and Semimetals. 1997; 47: 123-174.